Application of the Herschel-Quincke Tube Concept to Higher-Order Acoustic Modes in Two-Dimensional Ducts

Lori A. Brady

Thesis submitted to the Faculty of the
Virginia Polytechnic Institute and State University
in partial fulfillment of the requirements for the degree of

Master of Science
in
Mechanical Engineering

Ricardo A. Burdisso, Chair
Alfred W. Wicks
J. Kenneth Shaw

1 March 2002
Blacksburg, Virginia

Keywords: Acoustics, Noise Control, Duct, Herschel-Quincke Tubes, Higher-Order Modes, Green's Function

Application of the Herschel-Quincke Tube Concept to Higher-Order Acoustic Modes in Two-Dimensional Ducts

Lori A. Brady

(ABSTRACT)

The application of the Hershcel-Quincke (HQ) tube as a noise reduction device for one-dimensional plane-wave sound fields has been studied in great detail in previous years. In this thesis, an analytical technique is developed to investigate the potential of the HQ tube concept to control higher-order duct modes. This analytical method involves modeling the tube-duct interfaces as finite piston sources, which couple the acoustic field inside the main duct with the acoustic field within the HQ tube(s). The acoustic field within the HQ tube is modeled as plane-waves and the acoustic field within the main duct is modeled by expanding the sound field in terms of the higher-order modes. This model is then used to investigate the noise reduction mechanisms behind the attenuation of higher-order modes. These mechanisms involve both the reflection of the incident wave as well as the reconstruction and recombination of the modal content of the incident disturbance into other modes. The effects of the modal content of the disturbance along with the HQ tube geometric parameters, such as tube axial position, length, distance between interfaces, and cross-sectional area, are studied with respect to the frequencies of attenuation and the reduction obtained. These results show the potential of the Herschel-Quincke tube concept to reduce higher-order modes in ducts.

.

Author's Acknowledgements

First, I would like to thank my advisor Ricardo Burdisso for all of his guidance and support throughout this research and the writing of this thesis. Many thanks are also extended to Al Wicks and Ken Shaw for their support and contributions to this work and as graduate committee members.

I would like to acknowledge all of the administrative help I received from Dawn Bennett, Cathy Hill, Lynda King, and Eloise McCoy. Without them I would have been lost.

I am also thankful to all the members of the Vibration and Acoustics Laboratories (VAL). The support among its members and the friendships in the lab proved an invaluable asset in work presented here.

I am also grateful to the support of my family. I thank them for their love, encouragement, and patience.

Finally, I would like to thank the NASA Langley Research Center for their support of this research under grant NAG-1980 and my graduate studies. It is greatly appreciated.

Table of Contents

List of Figures

List of Tables

Chapter 1 - Introduction

1.1 Prologue

Duct acoustics is the study of the propagation of sound within a confined space. Given a certain noise source, the emitted sound will propagate with characteristics primarily dependent upon the surrounding duct geometry, acoustic properties of the boundary, and the frequency of excitation. A standard duct geometry is the infinite rigid-walled duct. The sound field within such a duct is composed of both standing waves in the transverse direction and traveling or evanescent waves in the longitudinal direction. At low frequencies, those below the first cut-off frequency of the system, the sound field is one-dimensional and only the plane-wave mode will propagate within the duct. At higher frequencies, above the first cut-off frequency, the sound field becomes more complex due to the presence of higher-order modes. These higher-order modes include both propagating and evanescent components [1].

There are many noise control strategies, which can be utilized to reduce noise in ducts. In general, noise control methods can be applied to the noise source, the transmission path, and/or the receiver. However, noise problems are often times only considered in pre-existing systems where many of these modifications can be difficult to implement due to inherent limitations [2]. In addition, noise control strategies can be characterized as active, passive, or a combination of both passive and active approaches.

Active noise control techniques in ducts consist of the introduction of secondary noise sources to either cancel, suppress, or absorb part of the original sound field [3]. This method typically involves using a digital processor which drives a set of secondary or control noise sources based on information gathered about the sound field from a set of sensors, i.e. microphones. Usually, the secondary sources will produce a sound field that is out of phase with the original field and noise cancellation occurs due to destructive interference. The number of secondary sources and sensors required is determined by the complexity of the original sound field and the magnitude of cancellation needed [4].

Passive noise control techniques in ducts generally consist of either the absorption or the reflection of the original sound field. Absorptive techniques consist of lining a duct with sound-absorbing materials, also called liners, as shown in Figure 1.1. These liners, which typically consist of porous materials like fiberglass or foam, react locally with the sound field and through friction attenuate sound energy through heat. Specific properties for these materials, which will determine its effectiveness in absorbing sound, include the thickness of the treatment, its density, and its acoustic impedance [5]. Generally speaking, the thickness of the sound absorbing material is related to the range of wavelengths able to be attenuated. With increasing thickness, a liner will be able to attenuate longer wavelengths, i.e. lower frequencies. For this reason, liners are normally used for high frequency broad-band disturbances, which consist of mainly higher-order modes.

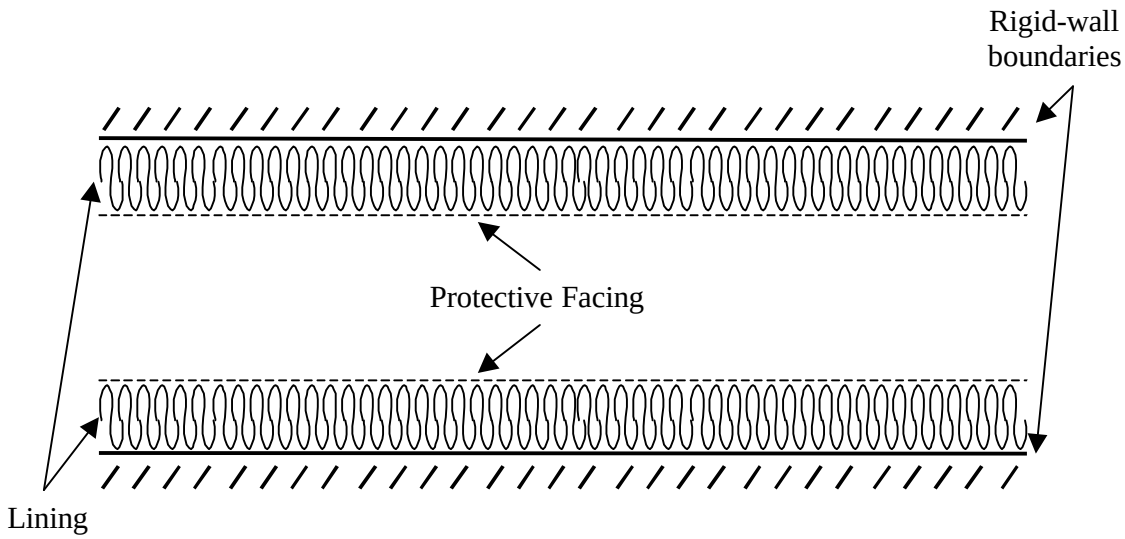

Figure 1.1. Passive acoustic liner in rigid-walled duct

Reactive techniques consist of changes in the duct geometry, which result in a reflection of part of the original sound field back toward the noise source. These reactive devices include, but are not limited to, expansion chambers, Helmholtz resonators, and Herschel Quincke tubes. All of these techniques are typically used for lower frequency disturbance applications, which consist of the plane-wave mode [6].

Both the expansion chamber and the Helmholtz resonator are shown in Figure 1.2. The expansion chamber, in Figure 1.2(a), is qualified as an acoustic low-pass filter, which is characterized by an enlarged section of duct. At low frequencies, the sound reduction is a function of the relative difference between the duct and expansion areas. The Helmholtz resonator, as shown in Figure 1.2(b), is used as an acoustic band-pass filter. Thus resonator creates a band of attenuation centered on a frequency which is depended upon the resonator volume, neck area, and neck length [7].

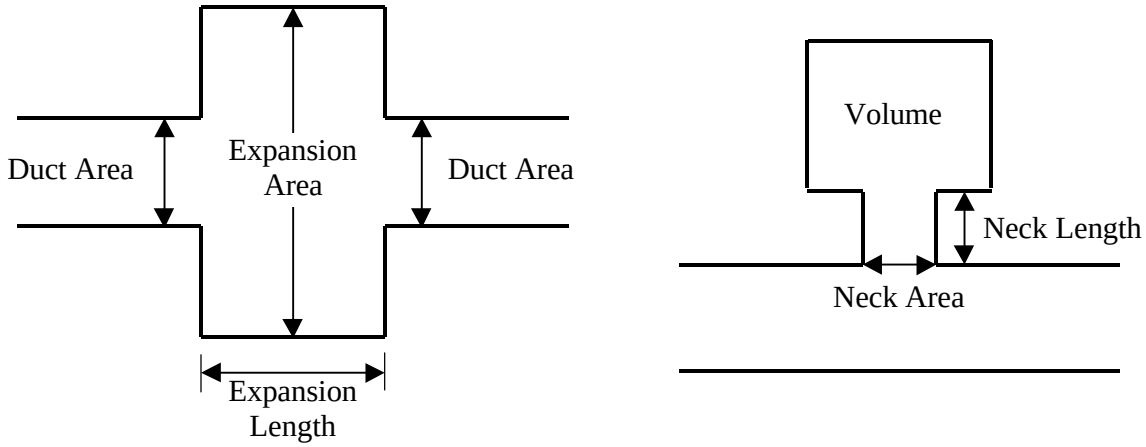

(a) Expansion chamber (b) Helmholtz resonator

Figure 1.2. Passive noise control devices – reactive type

A Herschel-Quincke (HQ) tube is essentially a hollow side-tube that travels along a main-duct axis and attaches to the main-duct at each of the two ends of the tube, as shown in Figure 1.3. In general, an incident plane-wave acoustic wave, traveling to the right, encounters a branch in the path at the first intersection of the side-tube and main-duct, named the inlet of the HQ tube. The incident wave divides and will later recombine at the second intersection of the side-tube and main-duct, similarly named the outlet of the HQ tube. A difference in path length will create a phase shift between the recombined signals and consequently attenuation of sound at a number of discrete frequencies. Changing tube parameters such as length (L), area (S), and the distance between inlet and outlet openings, termed the interface distance (ℓ), the frequencies of cancellation can be adjusted.

This thesis will investigate the HQ tube approach for the case of higher-order acoustic mode disturbances. This should be contrasted to previous studies of the HQ approach where only plane-waves were considered in the system.

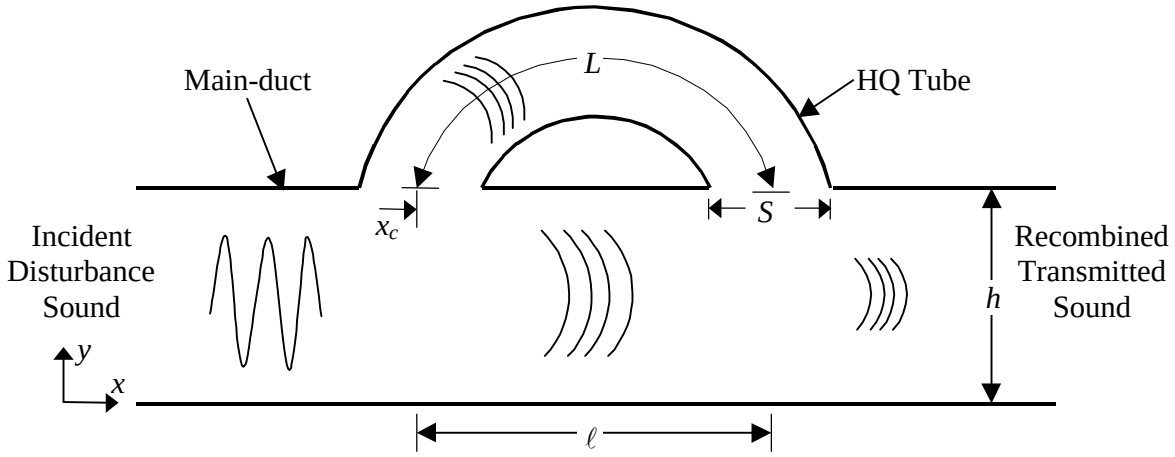

Figure 1.3. Herschel-Quincke tube concept

1.2 Review of Literature on Hershcel-Quincke Tube Concept

Herschel [8] first discussed the idea of acoustic interference of musical tones in such a system in 1833. He predicted that cancellation of tones would occur when the path length difference between the recombined signals was $(2m+1)(\lambda/2)$, where λ is the wavelength of the acoustic wave and m is any integer. Later, in 1866, Quincke [9] experimentally validated that Herschel's system did effectively cancel sound.

Stewart [10], in the 20th century, found Herschel's theoretical explanation to be insufficient to interpret experimental data he had observed. Using a plane-wave analysis, Stewart derived an analytical model describing the ratio of transmitted to incident sound intensity in the system. He verified that cancellation does occur when the path length difference is $(2m+1)(\lambda/2)$, as predicted by Herschel [8]. However, it was found that attenuation also occurs when the path length difference is $m\lambda$ with limited attenuation at other transitional frequencies.

Stewart's model assumed that the HQ tube system was composed of three duct sections, each with constant cross-sectional area. These three duct sections described; the entrance portion of the main-duct (up to the side-tube inlet), the HQ tube and section of main-duct between the HQ tube intersections, and the exit portion of the main duct (following the HQ tube outlet). The cross-sectional areas of the HQ tube and the section of main-duct between the HQ tube intersections were assumed to be equal. Although, Stewart's work was a valuable contribution in the analysis of HQ tubes, the model could only be used in the absence of flow and was still limited to plane wave acoustic fields.

Only recently did Selamet, et. al. [11, 12] extend Stewart's work by deriving an analytical model without the limitations on duct cross-sectional geometry. However this model still does not include flow or higher-order modes. It is interesting to mention that approximately 65 years passed between Stewart's and Selamet's publications. In fact, during this time period very little work was reported in the literature on the subject of HQ tubes.

Beyond generalizing Stewart's work, Selamet, et. al. [13-16] continued to develop the analysis of the HQ systems to include alternatives in both modeling approach and system geometry. In 1994, Selamet, et. al. [13] studied multi-dimensional effects, seen at main-duct and HQ tube interfaces, using one-dimensional finite difference and three-dimensional boundary element numerical approaches. It was found that both numerical schemes compared well with each other and with experimental data, indicating the one-dimensional behavior of the sound fields well below the first main-duct higher-order mode cut-off frequency. However, some non-planar or higher-order mode behavior was observed at the HQ tube inlet. Still, Selamet, et. al. [13] concluded that the main-duct side-tube interfaces did not contribute to any deviation from the one-dimensional plane-wave behavior.

In 1995, Selamet, et. al. [14] modeled several acoustic silencers, including the HQ tube system, using a one-dimensional time-domain numerical approach. This model incorporated nonlinear behavior by simulating unsteady compressible flow. The objective of the work was to compare the well known linearized acoustic theory with the numerical solution, assuming zero mean flow. In the case of the HQ tube, it was found that the numerical model correlated well

with acoustic theory in the lower half of the frequency range studied, but with increasing frequency some variation could be seen. However, this discrepancy was not explained and further validation of the model was suggested for a future paper with experimental data. They speculated that if proven, the potential for this modeling approach is substantial for the reason that now nonlinear flow disturbances, as seen in internal combustion engines, could be considered. However, no publication was found for the model validation.

In 1996, Selamet, et. al. [15] looked at the influence of an expansion chamber in the HQ side-tube using once again a plane-wave modeling approach, as shown in Figure 1.4. Typically, in a HQ tube system without an expansion section, it is possible to control the resonant frequencies simply by changing the length of the HQ tube. However, with the addition of an expansion chamber, it was found that substantial shifting of the resonances can occur by changing the distance of the expansion chamber to the HQ tubes. This can be useful in the design of a HQ tube system for a noise control application in which the side-branched tubes are constrained to a certain length.

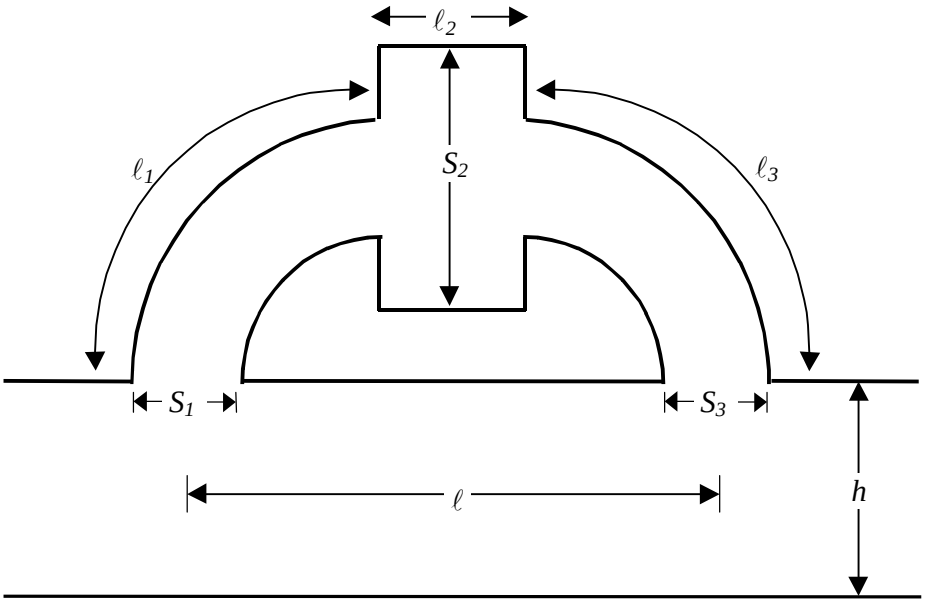

Figure 1.4. Herschel-Quincke tube with expansion chamber

In 1997, again Selamet, et. al. [16] published a paper considering yet another geometrical variation on the standard HQ tube system. This work extended the classical HQ tube system modeling to a multiple HQ tube configuration. It was found that with an increasing number of

HQ tubes the sound attenuation characteristics become more and more complicated. For this reason, numerical results were limited to two and three HQ tube arrangements. In general, it was found that the HQ tube diameter influences the width of transmission loss bands and HQ tube length influence system resonant frequencies. Also, it was shown that transmission loss characteristics for two and three HQ tube configurations differ greatly. More importantly, the intention of the paper was to simply present the modeling method for the multiple HQ tube system. This model can be valuable in determining the cost or benefit of an increasing number of HQ tubes for a specific noise control application.

Although these previous works produced a wealth of theoretical explanations of HQ tube systems for various geometric and modeling configurations, still the basic understanding is limited to systems with one-dimensional plane-wave sound fields. ***The influence of the HQ tube system on more complex acoustic fields has not as of yet been addressed.***

1.3 Objectives

There are two main objectives in this work. The first, is to develop an analytical model to address the effect of the HQ tubes when applied to a duct in the presence of a complex acoustic field, i.e. higher-order modes. The second is to determine the potential of the HQ tube system to suppress higher-order mode disturbances and the physical mechanisms responsible for this attenuation.

Specifically, the development of the theoretical model will attempt to accomplish several tasks. The first is to model the influence of the two-dimensional HQ system on higher-order mode acoustic fields. The second is to reevaluate the relevancy of classical one-dimensional HQ theory. Finally, this model will be used to gain insight into the physics behind the sound attenuation of higher-order modes. The realization of these objectives will benefit future work in the design of HQ tubes for practical noise reduction applications.

1.4 Outline of Thesis

The main goal of this thesis is to investigate the potential of the HQ tube system to suppress higher-order mode acoustic disturbances in two-dimensional ducts. Chapter 2 presents the analytical modeling technique developed to address the effect of the HQ tubes when applied to a duct in the presence of higher-order modes. This chapter also presents the extension of the basic system analysis to include HQ tubes in series, a comparison with the traditional plane wave acoustic theory, and various useful modeling simplifications.

In Chapter 3 numerical results are presented, in the form of parametric studies, to identify and explain the physical mechanisms behind the attenuation of higher-order modes. Various changes to the modal components of the disturbance and HQ tube geometry will be investigated. Changes in the modal components of the disturbance will consist of increasing the modal complexity of the disturbance while examining the system transmission loss characteristics. Modifications to the tube geometry will include changes in tube axial locations, lengths, interface distances, cross-sectional areas, and the addition of a second pair of HQ tubes.

Finally, in Chapter 4, the conclusions for the thesis are presented. The theory of the HQ tube systems, incorporating higher-order mode acoustic disturbances, is reviewed. The main conclusions are described and recommendations are made for future research and applications of this modeling technique and the HQ tube for noise control applications.

Chapter 2 – Analytical Modeling

In this chapter, the theoretical analysis for the two-dimensional HQ tube system is presented. This analytical model is desired in order to explore the physical mechanisms behind the attenuation of sound and to investigate how changes in geometric parameters influence this attenuation. Of primary consideration is developing a set of equations that describes the sound field within the duct due to a known higher-order mode disturbance and modified by the presence of the HQ tubes. This is accomplished using a Green's function technique assuming that the interfaces of the duct and tubes can be modeled as finite piston sources.

This analysis is presented for both a single pair of HQ tubes and for two pairs of HQ tubes in series. It should be kept in mind that the single-pair system is considered the primary system of interest and is modeled in detail. The system including two HQ tube pairs in series is simply an extension of the basic single-pair system model. In addition, the analysis will be extended to include several closed form theoretical results which allows for a direct comparison with the traditional plane-wave analysis. Also, it will be shown how to predict frequencies at which maximum attenuation will occur including the prediction of attenuation at the mode cut-off frequencies.

2.1 Hershcel-Quincke Tube System Concept

A disturbance noise field is assumed to propagate within a two-dimensional duct of height h in the positive x-direction. The pressure due to the disturbance can be found assuming that the system can be modeled as an infinite rigid-walled duct as shown below in Figure 2.1.

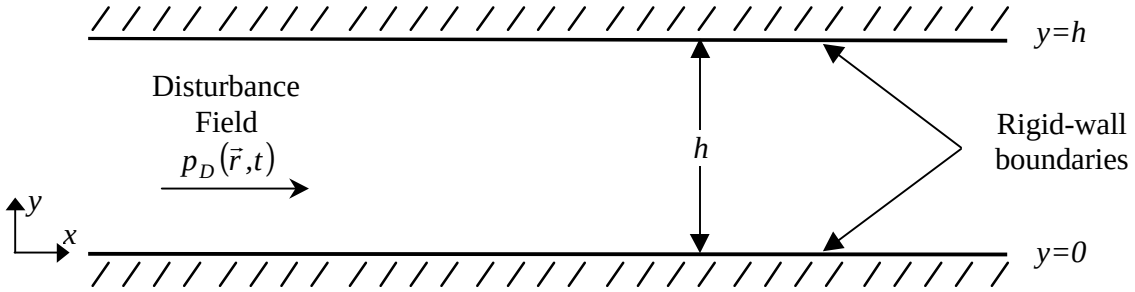

Figure 2.1. Simplified duct model - two-dimensional infinite duct

The pressure due to the disturbance, p_D, at any point in the duct, $\vec{r} = (x, y)$, can be expressed as the sum of a set of N_D modes of order m propagating in the positive direction. That is:

$$p_D(\vec{r}, t) = \sum_{m=0}^{N_D} A_m F_m(k_m y) e^{i(wt - k_x x)} \tag{2.1}$$

where A_m is the known complex amplitude of the m^{th} mode (with $m=0$ representing the plane-wave mode), $F_m(.)$ is the eigenfunction or duct mode, and k_m is the eigenvalue given as:

$$F_m(k_m y) = \cos(k_m y) \quad ; \quad k_m = \frac{mp}{h} \tag{2.2a,b}$$

In Figure 2.2, the eigenfunctions are plotted for modes $m=0$, *1*, *2*, *3*, and *4*, respectively. The positive and negative signs represent the instantaneous positive and negative acoustic pressure fluctuations.

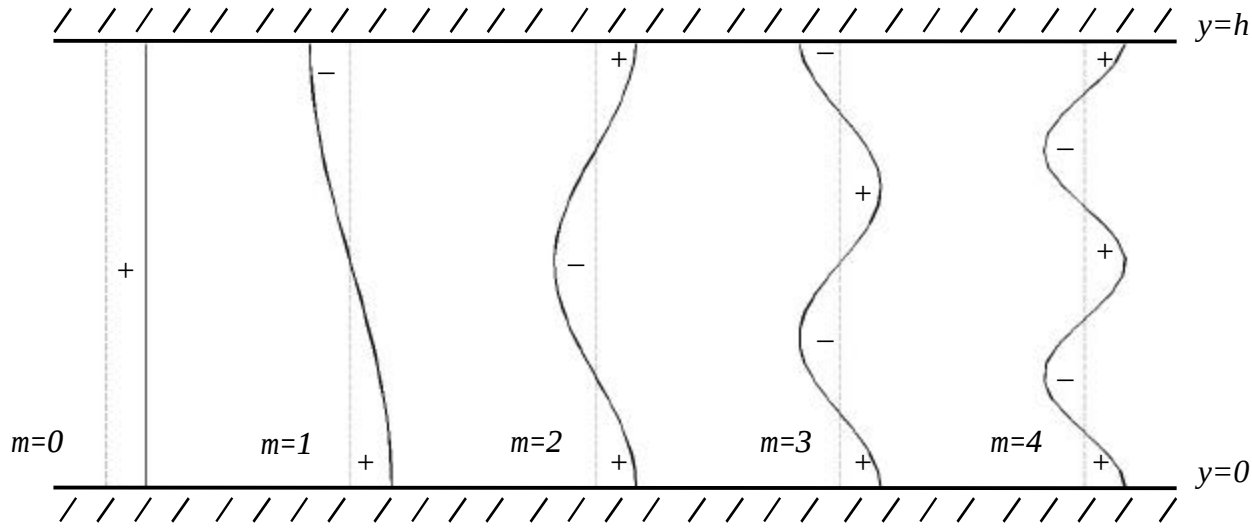

Figure 2.2. Eigenfunctions $F(k_m y)$ for $m=0$, *1*, *2*, *3*, and *4*

The propagation characteristics of the modes are given by the axial wavenumber k_x, which is given by:

$$k_x = \begin{cases} \sqrt{k^2 - k_m^2}, & k > k_m \\ -i\sqrt{k_m^2 - k^2}, & k < k_m \end{cases} \tag{2.3a,b}$$

where $k=w/c$ is the free-field wavenumber and c is the speed of sound. A mode will propagate for $k>k_m$ and will decay when $k<k_m$. The frequency at which this change in propagation characteristic occurs is termed the cut-off frequency for mode m. It is given for $k = k_m$ yielding:

$$w_m\left(rad/s\right) = \frac{cp}{h}m\,, \quad m = 0,1,2,3... \tag{2.4}$$

In Equation (2.1), only propagating modes that satisfy the condition in Equation (2.3a) are assumed in the disturbance at each frequency. The derivation of the disturbance pressure distribution, as described above, is presented in more detail in Appendix A.

The Herschel-Quincke tube system consists of a two-dimensional infinite rigid-walled duct which is modified to incorporate two side-branched tubes, symmetrically located about the duct axis. These tubes are referred there as a pair of Herschel Quincke (HQ) tubes. Figure 2.3 shows the system with a single pair of HQ tubes mounted at both the top and bottom of the duct. For the sake of clarity and understanding the dynamics of the system, the HQ tubes are described in two dimensions. Two HQ tubes are used to take advantage of simplifications that can be made due to symmetries when incorporating higher-order modes. The tubes are assumed to be of constant cross-sectional area S, per unit width, and have centerline length L. The tubes axial position is defined by the coordinate x_c at the first tube-duct interface. The distance between the tube openings along the duct axis is denoted as ℓ.

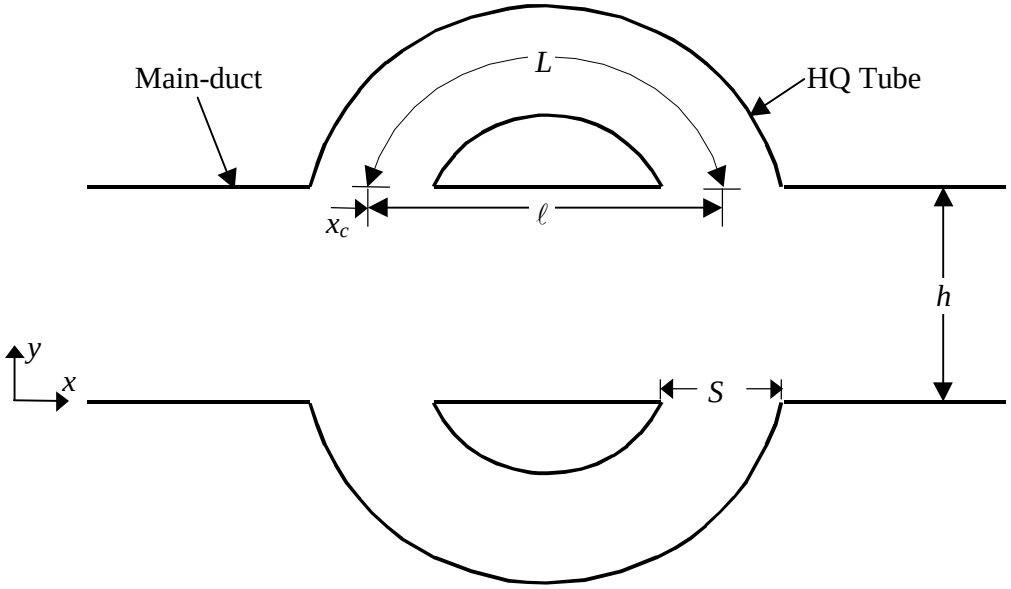

Figure 2.3. Herschel-Quincke tube modeling concept

The application of these HQ tubes as a noise reduction device has been previously studied in great detail, but for one-dimensional sound fields only, i.e. plane waves. The most recent theoretical treatment, for the basic HQ system with a plane-wave sound field, was derived by Selamet, et. al. [11]-[12] and for the sake of completeness is reproduced in Appendix B. However, these plane-wave models can not be used to investigate the performance of HQ tubes in the presence of higher-order modes. Thus, the main goal in this chapter is to develop models to study the noise reduction mechanisms of HQ tubes for higher-order modes.

The modeling of the HQ tube-duct system is carried out by first separating the HQ tubes from the duct at the interfaces, as shown in Figure 2.4. The models of the sound fields in the HQ tubes and in the main duct are first developed independently. Then, these models are fully coupled by matching the acoustic pressure and particle velocity at the tube-duct interfaces. The effect of the tubes on the duct is modeled by considering the tube-duct interfaces as finite piston sources radiating into the duct. Each piston is assumed to have an unknown velocity v^s (*s=1*, *2*, *3*, and *4*) which represents the particle velocities at the ends of the tubes. It is important to remark that, these piston sources can generate both plane-waves and higher-order modes in the duct.

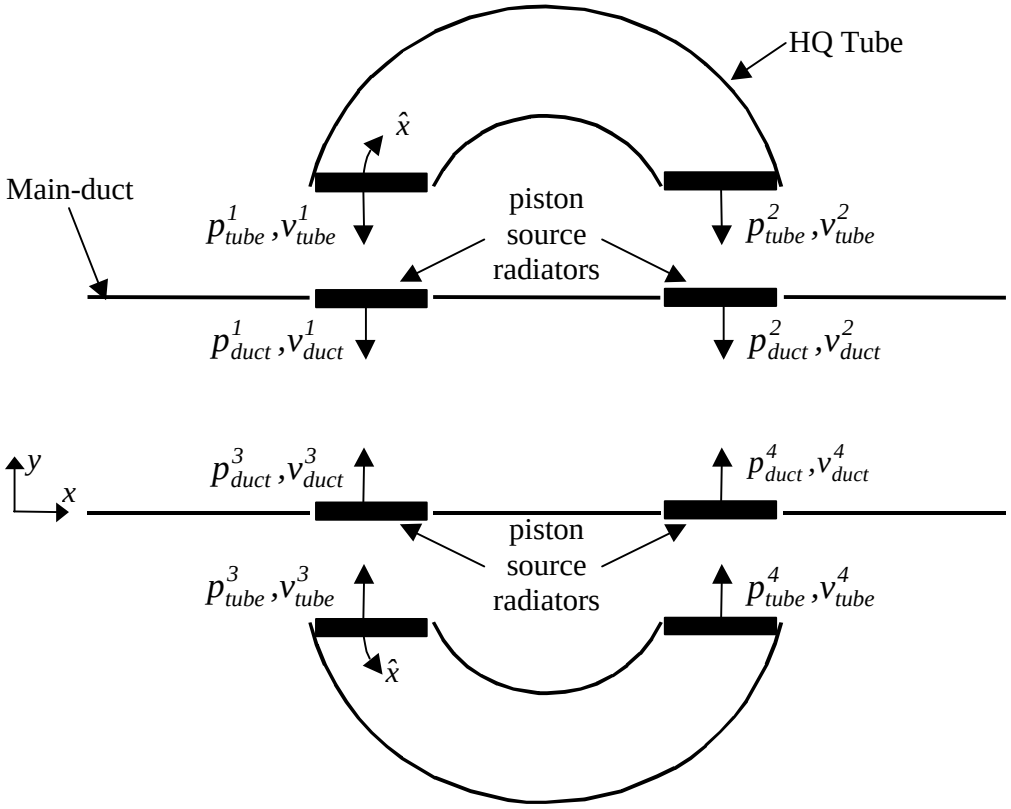

Figure 2.4. Uncoupled Herschel-Quincke system with finite piston source radiators

HQ Tube Model

In this study, the HQ tubes have been depicted as semi-circular in shape. However, for modeling purposes they are considered as straight tubes with uniform cross-sections, as shown in Figure 2.5. The sound fields inside the separated tubes are assumed to consist of plane-waves, i.e. there are no higher-order modes. This assumption is valid as long as the frequency range of interest is well below the first cut-off frequency of the HQ tubes. This upper limit frequency is defined as $f_{upper} = c/2S$.

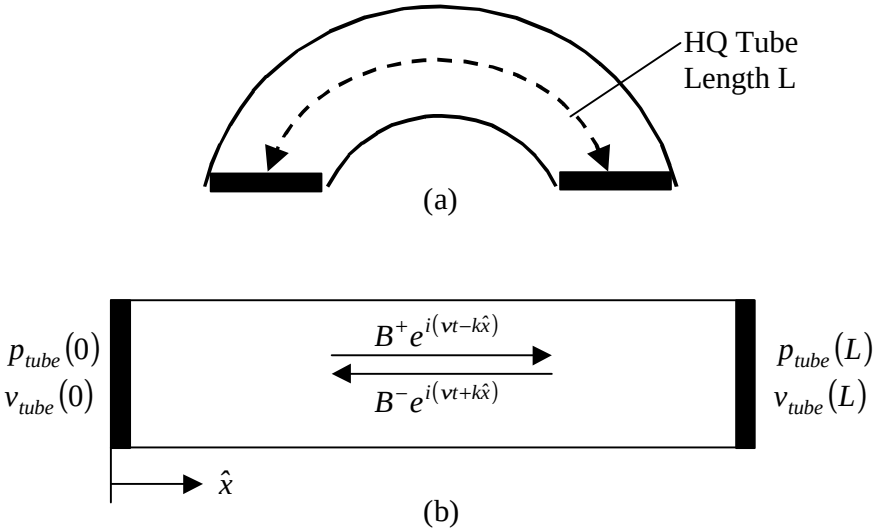

Figure 2.5. Uncoupled Herschel-Quincke tube with finite piston source radiators; (a) representation and (b) simplified model

The sound field inside the tube is given by:

$$p_{tube}(\hat{x},t) = B^+ e^{i(wt-k\hat{x})} + B^- e^{i(wt+k\hat{x})} \tag{2.5}$$

where B^+ and B^- represent the complex modal amplitudes of the plane-waves in the tube in the positive and negative propagating directions, respectively. The axial position within the HQ tube is denoted by the local coordinate $\hat{x}$.

The acoustic pressures and particle velocities at the ends of the tubes, i.e. $\hat{x}=0$ and $\hat{x}=L$, are expressed as:

$$p_{tube}(0,t) = \left(B^+ + B^-\right)e^{iwt} \quad p_{tube}(L,t) = \left(B^+e^{-ikL} + B^-e^{ikL}\right)e^{iwt} \tag{2.6a,b}$$

$$v_{tube}(0,t) = \frac{\left(B^+ - B^-\right)e^{iwt}}{rc} \quad v_{tube}(L,t) = \frac{\left(B^+e^{-ikL} - B^-e^{ikL}\right)e^{iwt}}{rc} \tag{2.6c,d}$$

where r is the fluid density, e.g. $r=1.2Ns^2/m^4$ in air at $20°C$. The acoustic pressure and particle velocity at the end of the tube can be expressed in matrix form as:

$$\begin{Bmatrix} p_{tube}(L) \\ v_{tube}(L) \end{Bmatrix} = \begin{bmatrix} \cos(kL) & irc\sin(kL) \\ \frac{-i}{rc}\sin(kL) & -\cos(kL) \end{bmatrix} \begin{Bmatrix} p_{tube}(0) \\ v_{tube}(0) \end{Bmatrix} \tag{2.7}$$

Rearranging Equation (2.7), the acoustic pressure at the end of the tube can be rewritten in terms of the velocity as:

$$\begin{Bmatrix} p_{tube}(0) \\ p_{tube}(L) \end{Bmatrix} = irc \begin{bmatrix} \cot(kL) & \csc(kL) \\ \csc(kL) & \cot(kL) \end{bmatrix} \begin{Bmatrix} v_{tube}(0) \\ v_{tube}(L) \end{Bmatrix} = [Z_{tube}] \begin{Bmatrix} v_{tube}(0) \\ v_{tube}(L) \end{Bmatrix} \tag{2.8}$$

where Z_{tube} represents the impedance matrix for the tube that relates the particle velocity to the pressure at the two ends of the tube. Equation (2.8) is valid for both of the HQ tubes in Figure 2.4. Thus, the relationship between the acoustic pressures and the particle velocities for both HQ tubes is conveniently written in matrix form as:

$$\begin{Bmatrix} \begin{bmatrix} p^1_{tube} \\ p^2_{tube} \end{bmatrix} \\ \begin{bmatrix} p^3_{tube} \\ p^4_{tube} \end{bmatrix} \end{Bmatrix} = \begin{bmatrix} [Z_{tube}] & 0 \\ 0 & [Z_{tube}] \end{bmatrix} \begin{Bmatrix} \begin{bmatrix} v^1_{tube} \\ v^2_{tube} \end{bmatrix} \\ \begin{bmatrix} v^3_{tube} \\ v^4_{tube} \end{bmatrix} \end{Bmatrix} \tag{2.9}$$

where the superscripts *1*, *2*, *3*, and *4* denote the four ends of the two tubes as indicated in Figure 2.4.

Duct Model with Finite Piston Sources and Disturbance

As depicted in Figure 2.6, the sound field in the separated main duct is obtained as the linear contribution of the sound due to the four piston sources and the disturbance. The pressure at an arbitrary point $\vec{r}$ in the main duct can be expressed as:

$$p_{duct}(\vec{r}) = \sum_{s=1}^{4} p_s(\vec{r}) + p_D(\vec{r}) \tag{2.10}$$

where $p_s(\vec{r})$ is the pressure due to the s^{th} piston source and $p_D(\vec{r})$ is the pressure due to the disturbance. The pressure due to the disturbance is given in Equation (2.1). On the other hand, the piston sources are assumed to move with unknown complex velocities, i.e. v_{duct}^{s} is the velocity of the s^{th} piston. Thus, the sound field generated by the piston sources is required and it is obtained by integrating the rigid-walled Green's function for an infinite duct over the cross-section of the source [17]. That is:

$$p_s(\vec{r}) = iwrv_{duct}^{s} \int_{x_s-S/2}^{x_s+S/2} G(\vec{r}\,|\,\vec{r}_0)\,dx_0 \tag{2.11}$$

where x_s is the center coordinate of the s^{th} piston source. The Green's function $G(\vec{r}\,|\,\vec{r}_0)$ is defined as the pressure at any point, $\vec{r}$, due to a point source located at $\vec{r}_0$. This is derived in Appendix C and is given as:

$$G(\vec{r}\,|\,\vec{r}_0) = \frac{-i}{2}\sum_{n=0}^{N_g}\frac{F_n(k_n y)F_n(k_n y_0)}{L_n k_x} e^{-ik_x|x-x_0|} e^{iwt} \tag{2.12}$$

In Equation (2.12) the axial wavenumber k_x, eigenfunctions $F_n(.)$, and eigenvalues k_n are the same as given in Equations (2.2)-(2.3), but distinguished by the subscript n representing the modal order of the Green's functions. The orthogonalization constant, L_n, is h if $n=0$ (the plane-wave mode) and $h/2$ if $n>0$ (the higher-order modes) and N_g is the number of modes included in the Green's function. Note that in the Green's function in Equation (2.12) both propagating and evanescent modes are included. Thus, the effect of the "piston source" near-fields are included by the evanescent modes.

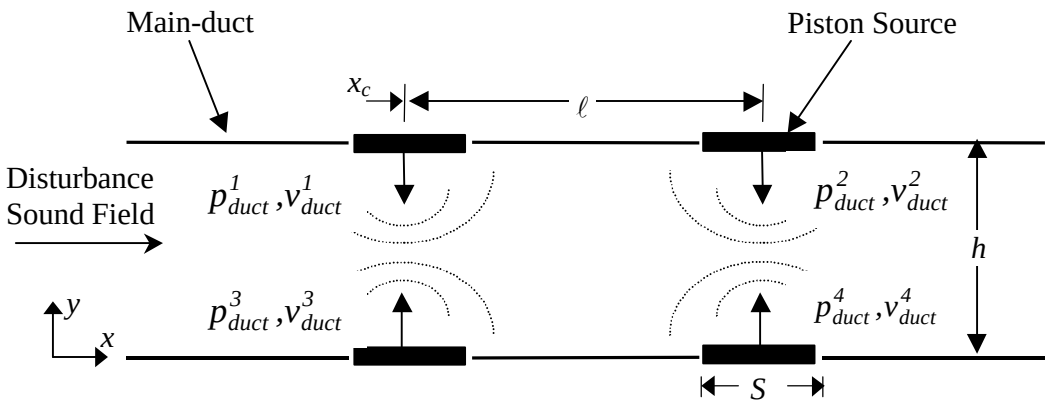

Figure 2.6. Uncoupled main-duct with finite piston source radiators

Once the piston velocities are found, the acoustic pressure anywhere in the main-duct can now be computed using the expressions in Equations (2.1), (2.10), and (2.11). To this end;

(i) the pressure and particle velocity at the interface between the HQ tubes and the main-duct need to be matched. Thus, the average pressure over the piston sources will be matched to the uniform pressure

and

(ii) the piston velocity will be matched to the particle velocity at the ends of the tubes, respectively.

Using Equation (2.10), the average acoustic pressure over the pistons can be expressed in matrix form as:

$$\begin{Bmatrix} p^1_{duct} \\ p^2_{duct} \\ p^3_{duct} \\ p^4_{duct} \end{Bmatrix} = iwr \begin{bmatrix} \tilde{\tilde{G}}_{11} & \tilde{\tilde{G}}_{12} & \tilde{\tilde{G}}_{13} & \tilde{\tilde{G}}_{14} \\ \tilde{\tilde{G}}_{21} & \tilde{\tilde{G}}_{22} & \tilde{\tilde{G}}_{23} & \tilde{\tilde{G}}_{24} \\ \tilde{\tilde{G}}_{31} & \tilde{\tilde{G}}_{32} & \tilde{\tilde{G}}_{33} & \tilde{\tilde{G}}_{34} \\ \tilde{\tilde{G}}_{41} & \tilde{\tilde{G}}_{42} & \tilde{\tilde{G}}_{43} & \tilde{\tilde{G}}_{44} \end{bmatrix} \begin{Bmatrix} v^1_{duct} \\ v^2_{duct} \\ v^3_{duct} \\ v^4_{duct} \end{Bmatrix} + \begin{Bmatrix} p^1_D \\ p^2_D \\ p^3_D \\ p^4_D \end{Bmatrix} = [Z_s] \begin{Bmatrix} v^1_{duct} \\ v^2_{duct} \\ v^3_{duct} \\ v^4_{duct} \end{Bmatrix} + \begin{Bmatrix} p^1_D \\ p^2_D \\ p^3_D \\ p^4_D \end{Bmatrix} \tag{2.13}$$

where p^s_{duct} is the average pressure over the s^{th} piston due to the disturbance and all four piston sources and Z_s is an impedance matrix that relates the piston source velocities to the average pressure over the sources. Thus, the average pressure over the s^{th} piston can be written as:

$$p^s_{duct} = iwr \sum_{s'=1}^{4} \tilde{G}_{rs} v^s_{duct} + p^s_D \tag{2.14}$$

The $\tilde{G}_{rs}$ element of the impedance matrix Z_s, in Equation (2.14), represents the average pressure over the r^{th} piston source due to a unit velocity of the s^{th} piston source. To derive this function, the pressure from Equation (2.11) due to the s^{th} piston needs to be integrated over the surface of the r^{th} piston. From the symmetry of the problem in Figure 2.7, there are only two cases to consider, which are presented in Appendix C. The elements of the Z_s matrix are given as:

$$\begin{aligned} \tilde{G}_{rs} &= \sum_{n=0}^{N_g} \frac{F(k_n y_r) F(k_n y_s)}{L_n k_x^2} \left(e^{-ik_x \frac{s}{2}} - 1 \right), \quad x_r = x_s \\ \tilde{G}_{rs} &= -i \sum_{n=0}^{N_g} \frac{F(k_n y_r) F(k_n y_s)}{L_n k_x^2} e^{-ik_x \ell} \sin\left(k_x \frac{s}{2} \right), \quad x_r \neq x_s \end{aligned} \tag{2.15}$$

and are illustrated in Figure 2.7.

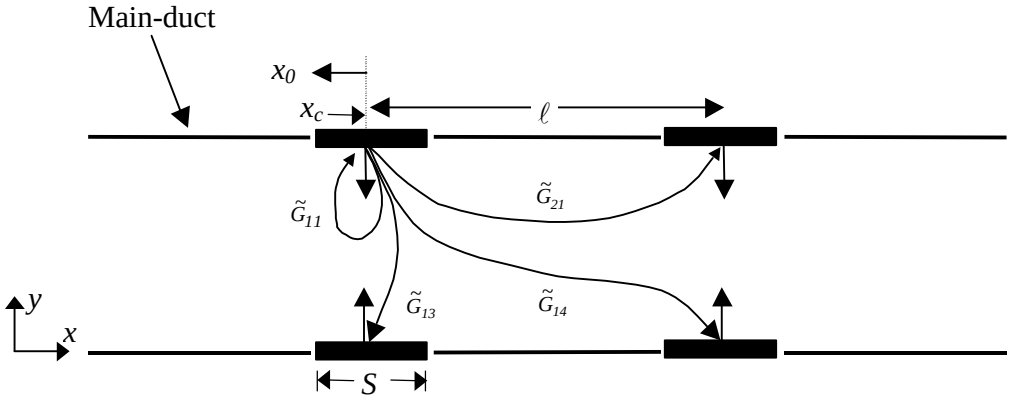

Figure 2.7. Samples of the integrated Green's functions

HQ Tube-Duct Coupling

Figure 2.8 shows the coupled system. The models for the HQ tubes and the main-duct are coupled by matching (i) the pressure on the surface of the pistons to the constant pressure at the end of the HQ tube and (ii) the piston velocity to the particle velocity at the end of the HQ tube, i.e. $p^s_{tube} = p^s_{duct}$ and $v^s_{tube} = v^s_{duct}$, for *s=1, 2, 3,* and *4* (see Figure 2.4). Replacing v^s_{tube} by v^s_{duct} in Equation (2.9) and substituting this into Equation (2.13) leads to a linear system of equations that can be solved for the unknown piston source velocities, v^s_{duct}. That is:

$$\begin{Bmatrix} v^1_{duct} \\ v^2_{duct} \\ v^3_{duct} \\ v^4_{duct} \end{Bmatrix} = \left(\begin{bmatrix} [Z_{tube}] & 0 \\ 0 & [Z_{tube}] \end{bmatrix} - [Z_s] \right)^{-1} \begin{Bmatrix} p^1_D \\ p^2_D \\ p^3_D \\ p^4_D \end{Bmatrix} \tag{2.16}$$

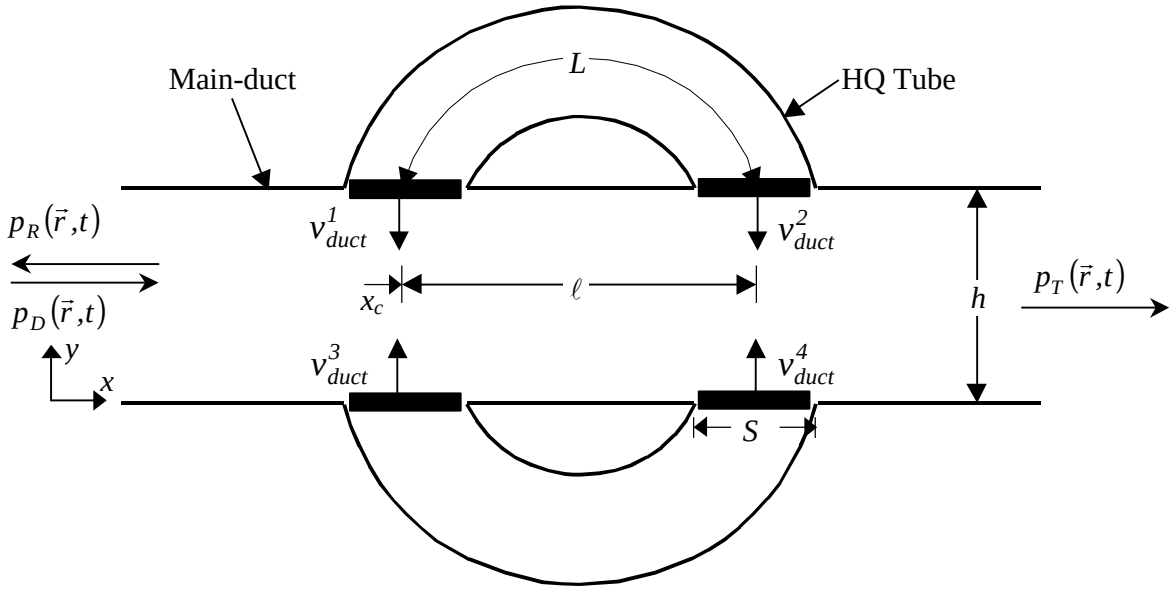

Figure 2.8. Coupled Hershcel-Quincke system

Once the source velocities are known, the pressure at any location within the duct can be found using Equation (2.10). It is conveinent to express the pressure within the duct in terms of the disturbance, transmitted, and reflected modal amplitudes as depicted in Figure 2.8. The

modal amplitude of the disturbance is given in Equation (2.1), i.e. A_m. The modal amplitudes of both the transmitted and reflected waves are found using Equation (2.10). The transmitted pressure is defined at $x \geq x_c + \ell$ and is given as:

$$p_T(x,y) = \sum_{s=1}^{4} p_s^T(x,y) + p_D(x,y), \quad \begin{matrix} x \geq x_c + \ell \\ 0 \leq y \leq h \end{matrix} \tag{2.17}$$

where p_s^T is the transmitted acoustic pressure due to the s^{th} piston. Adding the contributions of the four piston sources and the disturbance, the transmitted sound field is given as:

$$p_T(x,y) = \left\{ wr \sum_{n=0}^{N_g} \frac{\sin\left(k_x \frac{s}{2}\right)}{L_n k_x^2} e^{ik_x x_c} \left[\left(v_{duct}^1 + v_{duct}^2 e^{ik_x \ell} \right) \cos(k_n h) + \left(v_{duct}^3 + v_{duct}^4 e^{ik_x \ell} \right) \right] \right\} \cos(k_n y) e^{i(wt - k_x x)} + \left\{ \sum_{m=0}^{N_D} A_m \right\} \cos(k_m y) e^{i(wt - k_x x)} \tag{2.18}$$

where the velocity terms are obtained from Equation (2.16). Thus, the modal amplitude of the transmitted n^{th} modes is given as:

$$A_{Tn} = wr \frac{\sin\left(k_x \frac{s}{2}\right)}{L_n k_x^2} e^{ik_x x_c} \left[\left(v_{duct}^1 + v_{duct}^2 e^{ik_x \ell} \right) \cos(k_n h) + \left(v_{duct}^3 + v_{duct}^4 e^{ik_x \ell} \right) \right] + A_n, \quad \begin{matrix} n = 1,\ldots,N_g \\ x > x_c + \ell \end{matrix} \tag{2.19}$$

Similarly, the reflected pressure distribution is defined at $x < x_c$ and is given as:

$$p_R(x,y) = \sum_{s=1}^{4} p_s^R(x,y), \quad \begin{matrix} x < x_c \\ 0 \leq y \leq h \end{matrix} \tag{2.20}$$

that leads to:

$$p_R(x,y) = \left\{ wr \sum_{n=0}^{N_g} \frac{\sin\left(k_x \frac{s}{2}\right)}{L_n k_x^2} e^{-ik_x x_c} \left[\left(v_{duct}^1 + v_{duct}^2 e^{-ik_x \ell} \right) \cos(k_n h) + \left(v_{duct}^3 + v_{duct}^4 e^{-ik_x \ell} \right) \right] \right\} \cos(k_n y) e^{i(wt + k_x x)} \tag{2.21}$$

where the velocity terms are again obtained from Equation (2.16). Thus, the modal amplitude of the reflected modes is given as:

$$A_{Rn} = wr\,\frac{\sin\left(k_x\,\frac{s}{2}\right)}{L_n k_x^2} e^{-ik_x x_c}\left[\left(v_{duct}^{1} + v_{duct}^{2} e^{-ik_x \ell}\right)\cos(k_n h) + \left(v_{duct}^{3} + v_{duct}^{4} e^{-ik_x \ell}\right)\right], \quad \begin{matrix} n = 1,\ldots,N_g \\ x < x_c \end{matrix} \tag{2.22}$$

Using the modal amplitudes of the disturbance, transmitted, and reflected pressure distribution, the performance of the HQ tube system will be studied. The effectiveness of the HQ tubes as a noise control device is determined using the transmission loss (TL) as a metric. The TL is defined as a ratio of the disturbance to transmitted power as:

$$TL = 10\log_{10}\frac{P_D}{P_T} \tag{2.23}$$

Power is the rate at which energy flows through the duct axially and is given as the acoustic intensity in the x-direction integrated across the duct cross-section:

$$P = \int_0^h I_x(\vec{r})\,dy \tag{2.24}$$

where the intensity is defined as:

$$I_x(\vec{r}) = \frac{1}{2}\,real\left[p_x(\vec{r})\,v_x(\vec{r})^*\right] \tag{2.25}$$

and the notation * indicates the complex conjugate. The particle velocity is defined using Euler's equation and in the axial direction is given as:

$$v_x(\vec{r}) = -\frac{1}{iwr}\frac{\partial p_x(\vec{r})}{\partial x} \tag{2.26}$$

Thus, the expression for transmitted power in Equation (2.24) can be rewritten in terms of the disturbance, transmitted, and reflected modal amplitudes:

$$P_D = \frac{1}{2wr} real\left(k_x^*\right)\left|A_m\right|^2 L_m$$

$$P_T = \frac{1}{2wr} real\left(k_x^*\right)\left|A_{Tn}\right|^2 L_n \qquad \text{(2. 27a,b,c)}$$

$$P_R = -\frac{1}{2wr} real\left(k_x^*\right)\left|A_{Rn}\right|^2 L_n$$

where the modal amplitudes A_m, A_{Tn}, and A_{Rn} are defined in Equation (2.1), Equation (2.19), and Equation (2.22) respectively.

2.2 Herschel-Quincke Tubes in Series

The previously described model for the single pair of HQ tubes served the purpose of describing the modeling approach in detail. To extend the model to multiple pairs of HQ tubes, the same approach is taken. This analysis is undertaken to study whether multiple pairs have significant attenuation benefits over a single pair system.

The infinite duct is modified to incorporate two sets of HQ tube pairs, placed in series as shown in Figure 2.9. The first pair of tubes has the same configuration as the single-pair system described in Section 2.1. The second pair of HQ tubes is again assumed to be of constant cross-sectional area S_2 and centerline length L_2. The tubes are positioned axially at a distance x_{c2} from the outlets of the first pair. The distance between the tube openings along the duct axis is denoted as ℓ_2.

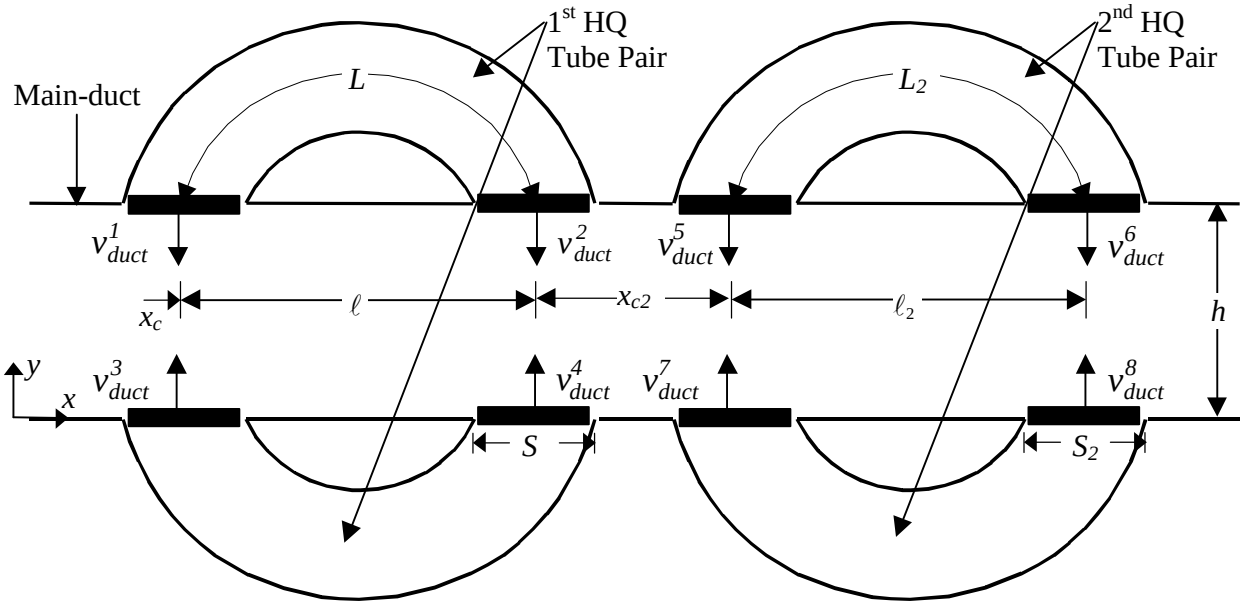

Figure 2.9. Herschel-Quincke tubes in series

The modeling approach is identical to the method used for the single-pair system. The modeling is carried out by first separating the HQ tubes from the duct at the interfaces. The models for the sound fields in the HQ tubes and in the main duct are first developed independently. Then, these models are fully coupled by matching both the pressure and particle velocity at the HQ tube and main-duct interfaces. The effect of the tubes on the duct is modeled by considering the tube-duct interfaces as finite piston sources radiating into the duct. Each piston is assumed to have an unknown velocity v_{duct}^{s} (*s = 1 through 8*) which represents the particle velocities at the ends of the tubes. These piston sources can generate both plane-waves and higher-order modes inside the duct.

The pressure distribution within the HQ tubes is assumed to consist of only plane-waves as expressed by Equation (2.5). Thus, once again, the sound field within the main duct is given as the summation of the pressure from the eight piston sources and the disturbance. That is:

$$p_{duct}(\vec{r}) = \sum_{s=1}^{8} p_s(\vec{r}) + p_D(\vec{r}) \tag{2.28}$$

where the pressure due to the disturbance p_D is evaluated using Equation (2.1) and the pressure due to a finite piston source is again obtained by integrating the rigid-walled Green's function for an infinite duct, as described in both section 2.1 and Appendix C.

Once the sound fields within the separated HQ tubes and main duct are defined, the coupling of these sound fields is accomplished by matching both pressure and particle velocity at the interfaces. The piston velocities are now attained as:

$$\begin{Bmatrix} v_{duct}^{1} \\ \vdots \\ v_{duct}^{8} \end{Bmatrix} = irc\left[\left[\begin{array}{c|c} TD_I & TD_{II} \\ \hline TD_{II} & TD_I \end{array}\right] - 2k\left[\begin{array}{c|c} \tilde{G}_{I,I} & \tilde{G}_{I,II} \\ \hline \tilde{G}_{II,I} & \tilde{G}_{II,II} \end{array}\right]\right]^{-1} \begin{Bmatrix} p_D^1 \\ \vdots \\ p_D^8 \end{Bmatrix} \tag{2.29}$$

where the sub-matrices for the HQ tube dynamics are given by:

$$TD_I = \begin{bmatrix} [y] & [0] \\ [0] & [y] \end{bmatrix} \quad TD_{II} = \begin{bmatrix} [z] & [0] \\ [0] & [z] \end{bmatrix} \tag{2.30}$$

and the matrices Y and z are given by:

$$y = \begin{bmatrix} cot(kL) & csc(kL) \\ csc(kL) & csc(kL) \end{bmatrix} \qquad z = \begin{bmatrix} cot(kL_2) & csc(kL_2) \\ csc(kL_2) & csc(kL_2) \end{bmatrix} \tag{2.31}$$

The second matrix in Equation (2.29) is defined as:

$$\tilde{G}_{I,I} = \begin{bmatrix} \tilde{G}_{11} & \tilde{G}_{12} & \tilde{G}_{13} & \tilde{G}_{14} \\ \tilde{G}_{21} & \tilde{G}_{22} & \tilde{G}_{23} & \tilde{G}_{24} \\ \tilde{G}_{31} & \tilde{G}_{32} & \tilde{G}_{33} & \tilde{G}_{34} \\ \tilde{G}_{41} & \tilde{G}_{42} & \tilde{G}_{43} & \tilde{G}_{44} \end{bmatrix} \quad \tilde{G}_{I,II} = \begin{bmatrix} \tilde{G}_{15} & \tilde{G}_{16} & \tilde{G}_{17} & \tilde{G}_{18} \\ \tilde{G}_{25} & \tilde{G}_{26} & \tilde{G}_{27} & \tilde{G}_{28} \\ \tilde{G}_{35} & \tilde{G}_{36} & \tilde{G}_{37} & \tilde{G}_{38} \\ \tilde{G}_{45} & \tilde{G}_{46} & \tilde{G}_{47} & \tilde{G}_{48} \end{bmatrix}$$
$$\tilde{G}_{II,I} = \begin{bmatrix} \tilde{G}_{51} & \tilde{G}_{52} & \tilde{G}_{53} & \tilde{G}_{54} \\ \tilde{G}_{61} & \tilde{G}_{62} & \tilde{G}_{63} & \tilde{G}_{64} \\ \tilde{G}_{71} & \tilde{G}_{72} & \tilde{G}_{73} & \tilde{G}_{74} \\ \tilde{G}_{81} & \tilde{G}_{82} & \tilde{G}_{83} & \tilde{G}_{84} \end{bmatrix} \quad \tilde{G}_{II,II} = \begin{bmatrix} \tilde{G}_{55} & \tilde{G}_{56} & \tilde{G}_{57} & \tilde{G}_{58} \\ \tilde{G}_{65} & \tilde{G}_{66} & \tilde{G}_{67} & \tilde{G}_{68} \\ \tilde{G}_{75} & \tilde{G}_{76} & \tilde{G}_{77} & \tilde{G}_{78} \\ \tilde{G}_{85} & \tilde{G}_{86} & \tilde{G}_{87} & \tilde{G}_{88} \end{bmatrix} \tag{2.32}$$

where the sub-indices I and II denote associations with the first and second HQ tube pairs respectively. Therefore, as an example the elements of matrix $\tilde{G}_{I,II}$ represent the average pressure over the piston sources of the first HQ tube pair due to a unit velocity of pistons on the second HQ tube pair.

Once the source velocities are known, the pressure at any location within the duct can be found using Equation (2.28). Again, it is convenient to express the pressure within the duct in terms of the disturbance, transmitted, and reflected modal amplitudes. The amplitude of the transmitted and reflected modes are given as:

$$A_{Tn} = wr\,\frac{e^{ik_x x_c}}{L_n k_x^2}\left[\begin{array}{l} sin\left(k_x\,\frac{s}{2}\right)\left[\left(v_1 + v_2 e^{ik_x \ell}\right)cos(k_n h) + \left(v_3 + v_4 e^{ik_x \ell}\right)\right] \\ + sin\left(k_x\,\frac{s_2}{2}\right)e^{ik_x(\ell + x_{c2})}\left[\left(v_5 + v_6 e^{ik_x \ell_2}\right)cos(k_n h) + \left(v_7 + v_8 e^{ik_x \ell_2}\right)\right] \end{array}\right] + A_n$$
$$A_{Rn} = wr \sum_{n=0}^{N_q} \frac{e^{-ik_x x_c}}{L_n k_x^2}\left[\begin{array}{l} sin\left(k_x\,\frac{s}{2}\right)\left[\left(v_1 + v_2 e^{-ik_x \ell}\right)cos(k_n h) + \left(v_3 + v_4 e^{-ik_x \ell}\right)\right] \\ + sin\left(k_x\,\frac{s_2}{2}\right)e^{-ik_x(\ell + x_{c2})}\left[\left(v_5 + v_6 e^{-ik_x \ell_2}\right)cos(k_n h) + \left(v_7 + v_8 e^{-ik_x \ell_2}\right)\right] \end{array}\right] \tag{2.33a,b}$$

where the equations are valid as long as $x>x_c+\ell+x_{c2}+\ell_2$ and $x<x_c$ for the transmitted and reflected wave amplitudes respectively.

2.3 Modeling Simplifications – Single HQ Tube Pair

The models developed in previous sections allow for the prediction of the reduction of noise in a duct for an arbitrary configuration of HQ tube pairs. The accuracy of the model depends on the number of modes to be included in the Green's function. However, it is interesting to derive simplified expressions that would allow for easier understanding of the physics as well as guide in preliminary design of the HQ tube system. In this section, simplified expressions are presented to accomplish these goals.

The first step is to take advantage of the reciprocity property of the impedance functions in the case of no fluid flow. That is:

$$\tilde{\tilde{G}}_{rs} = \tilde{\tilde{G}}_{sr} \tag{2.34}$$

which implies that the average pressure at piston *r* due to a piston source at *s* is equivalent to the pressure at piston *s* do to the piston source at *r*. In other words, it is the distance between the observation piston and source piston which characterizes the impedance. This results from the exponential term found in the Green's function, which is dependant upon the absolute value of the difference between the observation point and source location in the *x*-direction. In addition, it is clear that:

$$\tilde{\tilde{G}}_{11} = \tilde{\tilde{G}}_{22} = \tilde{\tilde{G}}_{33} = \tilde{\tilde{G}}_{44} \tag{2.35}$$

Also, due to the symmetric placement of the HQ tubes about the duct axis, the following simplifications can be made (see figure 2.8):

$$\tilde{\tilde{G}}_{12} = \tilde{\tilde{G}}_{34} \quad \tilde{\tilde{G}}_{13} = \tilde{\tilde{G}}_{24} \quad \tilde{\tilde{G}}_{14} = \tilde{\tilde{G}}_{23} \tag{2.36}$$

Considering all of the above simplifications, Equation (2.16) can be reduced to:

$$\begin{Bmatrix} v_{duct}^1 \\ v_{duct}^2 \\ v_{duct}^3 \\ v_{duct}^4 \end{Bmatrix} = irc\left[\begin{bmatrix} cot(kL) & csc(kL) & 0 & 0 \\ csc(kL) & cot(kL) & 0 & 0 \\ 0 & 0 & cot(kL) & csc(kL) \\ 0 & 0 & csc(kL) & cot(kL) \end{bmatrix} - k\begin{bmatrix} \tilde{\tilde{G}}_{11} & \tilde{\tilde{G}}_{12} & \tilde{\tilde{G}}_{13} & \tilde{\tilde{G}}_{14} \\ \tilde{\tilde{G}}_{12} & \tilde{\tilde{G}}_{11} & \tilde{\tilde{G}}_{14} & \tilde{\tilde{G}}_{13} \\ \tilde{\tilde{G}}_{13} & \tilde{\tilde{G}}_{14} & \tilde{\tilde{G}}_{11} & \tilde{\tilde{G}}_{12} \\ \tilde{\tilde{G}}_{14} & \tilde{\tilde{G}}_{13} & \tilde{\tilde{G}}_{12} & \tilde{\tilde{G}}_{11} \end{bmatrix}\right]^{-1} \begin{Bmatrix} p_D^1 \\ p_D^2 \\ p_D^3 \\ p_D^4 \end{Bmatrix} \quad (2.37)$$

where it is now only necessary to evaluate four impedance terms.

It is possible to further simply the previous equation by considering that the disturbance input consists of even and odd modes separately. Due to the symmetric location of the HQ tubes, if the disturbance is comprised of only even (odd) modes, the piston velocities at the same axial location will be in phase (out of phase) and of equal magnitude; i.e. $v_{duct}^1 = v_{duct}^3$ and $v_{duct}^2 = v_{duct}^4$ ($v_{duct}^1 = -v_{duct}^3$ and $v_{duct}^2 = -v_{duct}^4$). Therfore, the impedance elements can be further simplified as $\tilde{\tilde{G}}_{11} = \tilde{\tilde{G}}_{13}$ and $\tilde{\tilde{G}}_{12} = \tilde{\tilde{G}}_{14}$ ($\tilde{\tilde{G}}_{11} = -\tilde{\tilde{G}}_{13}$ and $\tilde{\tilde{G}}_{12} = -\tilde{\tilde{G}}_{14}$). Using this information, it is now only necessary to find two piston source velocities, either v_{duct}^1 and v_{duct}^2 or v_{duct}^3 and v_{duct}^4 to specify the entire system. Equation (2.37) can now be reduced to:

$$\begin{Bmatrix} v_{duct}^1 \\ v_{duct}^2 \end{Bmatrix} = irc\left[\begin{bmatrix} cot(kL) & csc(kL) \\ csc(kL) & cot(kL) \end{bmatrix} - 2k\begin{bmatrix} \tilde{\tilde{G}}_{11} & \tilde{\tilde{G}}_{12} \\ \tilde{\tilde{G}}_{12} & \tilde{\tilde{G}}_{11} \end{bmatrix}\right]^{-1} \begin{Bmatrix} P_D^1 \\ P_D^2 \end{Bmatrix} \quad (2.38)$$

where:

$$\tilde{\tilde{G}}_{11} = \sum_{n=0}^{N_g} \frac{F_n (k_n h)^2 \left(e^{-ik_x \frac{s}{2}} - 1 \right)}{L_n k_x^2} \qquad \tilde{\tilde{G}}_{12} = -i \sum_{n=0}^{N_g} \frac{F_n (k_n h)^2 e^{-ik_x \ell} \sin\left(k_x \frac{s}{2}\right)}{L_n k_x^2} \quad (2.39a,b)$$

The system of equations in Equation (2.38) can be solved in closed form and the expressions for the modal amplitudes of the disturbance, transmitted, and reflected waves can be obtained. They are:

$$A_{Dn} = A_m \tag{2.40}$$

for the disturbance,

$$A_{Tn} = 2wr\,\frac{\cos(k_n h)\sin\left(k_x \frac{s}{2}\right)}{L_n k_x^2} e^{ik_x x_c}\left(v_{duct}^1 + v_{duct}^2 e^{ik_x \ell}\right) + A_n, \quad x > x_c + \ell \tag{2.41}$$

for the transmitted, and

$$A_{Rn} = 2wr\,\frac{\cos(k_n h)\sin\left(k_x \frac{s}{2}\right)}{L_n k_x^2} e^{-ik_x x_c}\left(v_{duct}^1 + v_{duct}^2 e^{-ik_x \ell}\right), \quad x < x_c \tag{2.42}$$

for the reflected modes, where the two piston source velocities, v_{duct}^1 and v_{duct}^2, are given as:

$$\begin{aligned} v_{duct}^1 &= \frac{P_D^1\left(a - 2iwr\tilde{G}_{11}\right) - P_D^2\left(b - 2iwr\tilde{G}_{12}\right)}{\left(a - 2iwr\tilde{G}_{11}\right)^2 - \left(b - 2iwr\tilde{G}_{12}\right)^2} \\ v_{duct}^2 &= \frac{P_D^2\left(a - 2iwr\tilde{G}_{11}\right) - P_D^1\left(b - 2iwr\tilde{G}_{12}\right)}{\left(a - 2iwr\tilde{G}_{11}\right)^2 - \left(b - 2iwr\tilde{G}_{12}\right)^2} \end{aligned} \tag{2.43a,b}$$

where:

$$a = \frac{irc}{\tan(kL)} \qquad ; \qquad b = \frac{irc}{\sin(kL)} \tag{2.44a,b}$$

and the pressure due to the disturbance is defined using Equation (2.1). This simplified model will be used in a comparison with the plane-wave modeling approach, to predict the frequencies of maximum attenuation for individual modes, and to predict attenuation at the cut-off frequency for an individual mode.

Comparison with Plane-Wave Modeling Approach

The model developed here for the HQ tubes can be used to investigate any disturbance modal distribution, i.e. plane-wave and higher-order modes. Thus, the model should also be capable of predicting the response at frequencies below the first cut-off frequency where only the plane wave mode is present. The simplified model developed above will be used to predict, in closed form, the attenuation for the case of a plane wave mode in the disturbance. In addition, this expression will be compared to the traditional plane wave model.

The plane-wave analysis method for investigating the HQ tube is shown in Appendix B. For the sake of comparison, the higher-order mode model as derived in Section 2.1 can be simplified for direct comparison with the plane-wave model. Assuming no fluid flow, the ratio of the disturbance to transmitted wave amplitude for a single mode can be found using Equation (2.40) and Equation (2.41) as:

$$\frac{A_{Dn}}{A_{Tn}} = \frac{L_n k_x^2 \left(\left(a - 2iwr\tilde{G}_{11}\right)^2 - \left(b - 2iwr\tilde{G}_{12}\right)^2 \right)}{4wr\cos(k_n h)^2 \sin\left(k_x \frac{s}{2}\right)\left[\left(a - 2iwr\tilde{G}_{11}\right) - \left(b - 2iwr\tilde{G}_{12}\right)\cos(k_x \ell)\right]} + 1 \qquad (2.45)$$

This expression can be further simplified for the plane wave mode, by setting $n=0$, $k_x=k$, and $L_n=h$ giving:

$$\frac{A_{D0}}{A_{T0}} = \frac{hk^2 \left(\left(a - 2iwr\tilde{G}_{11}\right)^2 - \left(b - 2iwr\tilde{G}_{12}\right)^2 \right)}{4wr\sin\left(k \frac{s}{2}\right)\left[\left(a - 2iwr\tilde{G}_{11}\right) - \left(b - 2iwr\tilde{G}_{12}\right)\cos(k\ell)\right]} + 1 \qquad (2.46)$$

Additionally, it is assumed that the acoustic wavelength is much larger than that of the source dimension, $l >> S$. The harmonic function can then be approximated as:

$$\sin\left(k_x \frac{s}{2}\right) \cong k_x \frac{s}{2} \quad ; \quad \cos\left(k_x \frac{s}{2}\right) \cong 1 \qquad (2.47a,b)$$

Taking into account these approximations and evaluating $\tilde{G}_{11}$ and $\tilde{G}_{12}$ using Equation (2.39a,b) the ratio of the disturbance to transmitted wave amplitude for the plane wave mode is given by:

$$\frac{A_{D0}}{A_{T0}} = \frac{h\left(\left(a - \frac{rcS}{h}\right)^2 - \left(b - \frac{rcS}{h}e^{-ik\ell}\right)^2\right)}{2rcS\left[\left(a - \frac{rcS}{h}\right) - \left(b - \frac{rcS}{h}e^{-ik\ell}\right)\cos(k\ell)\right]} + 1 \tag{2.48}$$

and rearranging for comparison with the plane-wave model, as depicted in Appendix B, gives:

$$\frac{A_{D0}}{A_{T0}} = \left[\frac{4\left(\frac{1 - e^{-2ikL} + AR\left(1 + e^{-2ikL} - 2e^{-ik\ell}e^{-ikL}\right)}{\left(1 - e^{-2ik\ell}\right)\left(1 - e^{-2ikl_L}\right)}\right) + AR^2}{4\left(\frac{e^{-ik\ell}}{1 - e^{-2ik\ell}} + AR\frac{e^{-ikL}}{1 - e^{-2ikL}}\right)}\right] e^{-ik\ell} \tag{2.49}$$

where:

$$AR = \frac{2S}{h} \tag{2.50}$$

is known as the system area ratio. Using Equation (2.23), the TL for the plane wave mode can be written as:

$$TL = 10\log_{10}\left|\frac{A_{D0}}{A_{T0}}\right|^2 = \left|\frac{4\left(\frac{1 - e^{-2ikL} + AR\left(1 + e^{-2ikL} - 2e^{-ik\ell}e^{-ikL}\right)}{\left(1 - e^{-2ik\ell}\right)\left(1 - e^{-2ikl_L}\right)}\right) + AR^2}{4\left(\frac{e^{-ik\ell}}{1 - e^{-2ik\ell}} + AR\frac{e^{-ikL}}{1 - e^{-2ikL}}\right)}\right|^2 \tag{2.51}$$

Comparing this expression for TL to the expression derived in Appendix B using the traditional plane-wave analysis shows that the expressions are identical. Therefore, it is proven that the higher-order mode modeling approach is equivalent to the plane-wave approach when considering only the plane-wave mode in both the disturbance and Green's functions. Thus, the traditional plane-wave model is a special case of the higher-order model developed here.

Frequencies of Maximum Attenuation

Another useful application of the simplified model developed in Section 2.3 is that it can be used to predict the frequency of maximum attenuation for individual modes. Maximum attenuation is obtained when the numerator of the ratio of the transmitted to disturbance wave amplitudes is set equal to zero. This ratio is defined, using Equation (2.40) and Equation (2.41) as:

$$\frac{A_{T0}}{A_{D0}} = 4wr\,\frac{\cos(k_n h)^2\,\sin\left(k_x \frac{s}{2}\right)\left[\left(a-2iwr\tilde{G}_{11}\right)-\left(b-2iwr\tilde{G}_{12}\right)\cos(k_x \ell)\right]}{L_n k_x^2\left(\left(a-2iwr\tilde{G}_{11}\right)^2-\left(b-2iwr\tilde{G}_{12}\right)^2\right)}+1 \qquad (2.52)$$

Using again the approximation in Equation (2.47a,b) and setting the above equation to zero, the frequencies of optimum attenuation for the selected mode *n* is obtained. This leads to the following transcendental equation:

$$\sin(kL) = -\frac{2Sk}{L_n k_x}\sin(k_x \ell) \qquad (2.53)$$

The significance of this expression is that for a fixed set of HQ tube parameters, e.g. *L*, ℓ, and *S*, Equation (2.53) shows that each mode has a set of optimum frequencies of attenuation, which increases with increasing modal orders. The left hand side of the equation depends only on the tube length. The right hand side of this equation is a function of the tube cross-sectional area, distance between interfaces, and the modal order. Thus, the optimal frequency of attenuation is

different for each mode present in the duct. This is depicted in Figure 2.10 where the left and right hand side of equation (2.53) are plotted as a function of the frequency. For a given tube length, the left hand side function is a single curve shown in Figure 2.10 (black line). The right hand side of the equation depends on the mode axial wavenumber k_x. The curves for modes *0*, *1*, *2*, and *3* are shown in the figure. The frequency of optimum attenuation occurs when the left and right hand side curves intersects as shown in the figure. For the same mode, there are many frequencies where the curves intersects, i.e. roots of equation (2.53). It is also interesting to show that as the area of the HQ tube is reduced ($S \rightarrow 0$), the optimum frequency of attenuation approaches the natural frequencies of the HQ tube assuming pressure release boundary conditions, i.e. $kL=0$. It is also interesting to note that for the plane-wave mode, i.e. $n=0$ and $k_x=k$, Equation (2.53) is the same expression found by Selamet et. al. [11, 12] using the traditional plane-wave analysis. Numerical results using this equation will be presented in Chapter 3 of this thesis.

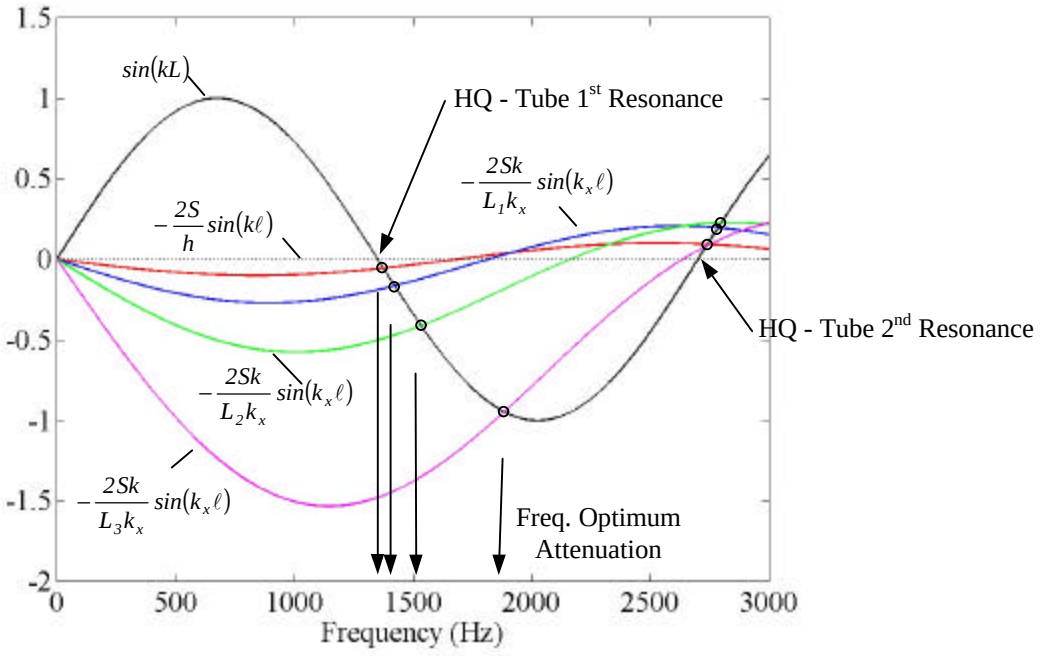

Figure 2.10. Single-mode frequencies of maximum attenuation

(*h=25.4 cm, S=1.27 cm, L=12.7 cm,* and ℓ*=10.16 cm*)

Attenuation at Mode Cut-Off Frequencies

Additionally, it is also of interest to note that the simplified model can also be used to predict attenuation at the cut-off frequency for an individual mode. This can be shown mathematically by looking at the limit of the transmitted to disturbance wave amplitude as the mode wavenumber approaches zero:

$$\lim_{k_x \to 0} \frac{A_{Tn}}{A_{Dn}} = 0 \tag{2.54}$$

where the ratio of transmitted to disturbance modal amplitude is given by Equation (2.52). Again assuming that that the acoustic wavelength is much larger than that of the source dimension, i.e. $l >> S$, and using the resulting approximations as stated in Equation (2.47a,b), this ratio is reduced to:

$$\lim_{k_x \to 0} \frac{A_{Tn}}{A_{Dn}} = \lim_{k_x \to 0} \left[2C \left[\frac{ak_x - bk_x - iC\ell k_x}{a^2 k_x^2 - 2Cak_x - b^2 k_x^2 + 2Cbk_x - 2iCb\ell k_x^2 + 2iC^2 \ell k_x + C^2 \ell^2 k_x^2} \right] + 1 \right] \tag{2.55}$$

where C is defined as:

$$C = \frac{wrS}{L_n} \tag{2.56}$$

The limit in Equation (2.55) is actually undefined because of the first term in the expression, i.e. $0/0$. This undefined term can be manipulated to obtain its limit using L'Hopital's rule [18]. L'Hopital's rule states that for a given ratio $f(x)/g(x)$, for which both $f(x_0)=0$ and $g(x_0)=0$, it can be shown that:

$$\lim_{x \to x_0} \frac{f(x)}{g(x)} = \lim_{x \to x_0} \frac{f'(x_0)}{g'(x_0)} \tag{2.57}$$

as long as *f(x)* and *g(x)* are continuous and have derivatives that are continuous on some open interval that contains x_0 . Equation (2.55) can now be reduced to:

$$\begin{aligned}\lim_{k_x \to 0} \frac{A_{Tn}}{A_{Dn}} &= 2C\left[\frac{a-b-iC\ell}{2a^2k_x - 2Ca - 2b^2k_x + 2Cb - 4iCb\ell k_x + 2iC^2\ell + 2C^2\ell^2 k_x}\right] + 1 \\ &= \left[\frac{a-b-iC\ell}{-a+b+iC\ell}\right] + 1 = 0\end{aligned} \tag{2.58}$$

where the ratio of transmitted to disturbance wave amplitude approaches zero in the limit as the wavenumber approaches zero. Thus, at the cut-off frequency the attenuation produced by the HQ tubes is perfect independent of the tube dimensions.

Chapter 3 – Numerical Analysis

In this chapter, the numerical analysis for the two-dimensional HQ tube system is presented. These numerical results are desired in order to explore the physical mechanisms behind the attenuation of sound, in particular the attenuation of higher-order acoustic modes. To accomplish this, it will be necessary to investigate how varying both the modal components of the disturbance and the system geometric parameters influence this attenuation. The HQ system transmission loss characteristics will be examined first with only a plane-wave disturbance, but this disturbance will be increased in complexity to include both even and odd higher-order modes. Also, the influence of geometric parameters such as tube axial position, length, distance between interfaces, cross-sectional area, and the number of tube arrays will be examined.

3.1 Modal Analysis with Increasing Disturbance Complexity

The following section describes the noise reduction mechanisms involved in the attenuation of high-order mode acoustic disturbances. This is accomplished by examining several aspects of the system characteristics by gradually increasing the modal complexity of the disturbance. The numerical results were computed for the two symmetrically located HQ tubes as shown in Figure 2.3. It was assumed that there was no fluid flow in the system, but that the fluid is air, i.e. $c=343$ *m/s* and $r=1.21$ Ns^2/m^4.

Comparison with Plane-Wave Modeling Approach

The first case investigated compares the simplified higher-order model developed in Section 2.3 for a plane-wave disturbance to the traditional plane-wave analysis by Selamet et. al. [10-11], which was reproduced in Appendix B. The dimensions of the system are $h=4.9$ cm, $S=2.45/2$ *cm*, $L=0.8$ *m*, and $\ell=0.4$ *m* for the higher-order mode model and the parameters for the plane-wave model are $S_d=4.9$ cm, $S_t=2.45$ *cm*, $\ell_3=0.8$ *m*, and $\ell_2=0.4$ *m*. The first cut-off frequency, i.e. $m=1$, is *3500 Hz*. For this comparison, several system characteristics will be investigated including, the frequencies of maximum attenuation, the phase relationship between the recombined waves at the outlet of the HQ tube, and the transmission loss.

Equation (2.53) is used to predict the frequencies of maximum attenuation assuming a single mode both in the disturbance and in the Green's function. This equation is best depicted by plotting the left and right-hand sides on the same plot, as is shown in Figure 2.10. The frequencies of maximum attenuation occur at the intersections of these curves. The significant of these results is that for a given set of system geometric parameters (*h, S, L,* and ℓ) each mode has a set optimum frequencies of attenuation, which increases with modal order.

This analysis can be taken a step further by investigating the phase relationship between the recombined waves. The phase relationship is easily explained using Figure 3.1. In this figure, the incident sound field, traveling to the right, encounters a branch in path at the inlet of the HQ tube. The incident wave then divides into the wave travelling through the HQ tube and the wave remaining in the main-duct. At this first intersection, it is assumed that all of the waves are in phase. Both of these divided waves travel and recombine at the outlet of the HQ tube. The waves in the HQ tube and main-duct travel a distance of *L* and ℓ respectively. Therefore, the relative phase between the recombined waves is defined as:

$$kL - k_x \ell \tag{3.1}$$

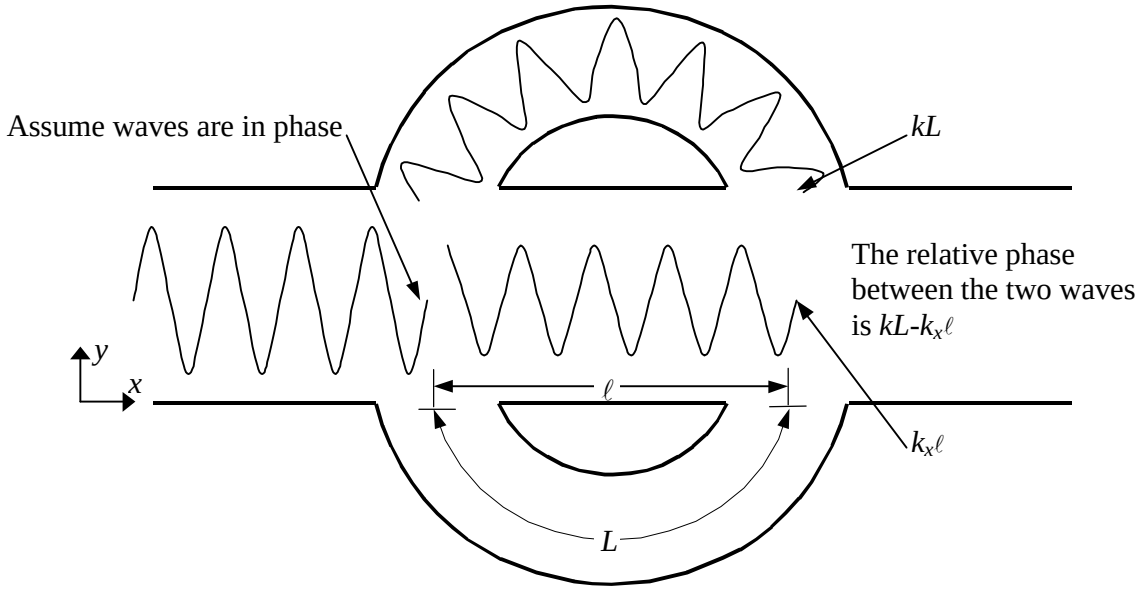

Figure 3.1. Phase relationship between recombined waves

Figure 3.2 shows these system characteristics over a frequency range below the first cut-off frequency, i.e. *3500 Hz*. The top subplot is the left and right-hand side of Equation (2.53), the center subplot is the phase difference between the recombined waves, and the bottom subplot is the transmission loss comparison between modeling approaches. The higher-order mode results were calculated assuming that only the plane-wave is present in the disturbance, but that the finite piston sources are capable of generating higher-order modes in the duct, i.e., the evanescent modes were included in the Green's functions or $N_g=129$.

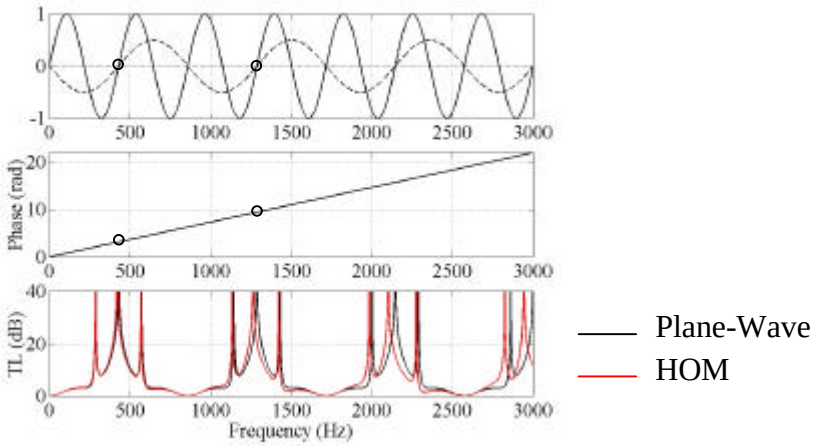

Figure 3.2. Comparison of plane-wave and higher-order mode models including; frequencies of maximum attenuation, phase difference of recombined waves (rad), and transmission loss (dB)

As seen in the top subplot of the previous figure, the frequencies of maximum attenuation occur at the intersections of the two sinusoidal curves. Two such intersections have been highlighted and occur at *421* and *1261 Hz*. At these frequencies the phase difference between the recombined waves are *3.1* and *9.4 rad*, corresponding to path length differences of *1/2* and *3 1/2*, respectively. Also of note is the increasing discrepancy with frequency between the plane-wave and higher-order mode transmission loss curves in the bottom subplot. The differences between the two curves are due to the inclusion of the near-field effects of the evanescent modes in the higher-order mode model. The effect of the evanescent modes becomes more significant as the frequency increases and approaches the cut-off frequency of the first higher-order mode. Thus, the traditional plane-wave approach is only valid at very low frequencies, well below the cut-off frequency of the *m=1* mode. When the evanescent modes, created by the finite piston

sources, are removed the plane-wave and the higher-order mode results are identical. In fact, it has been shown analytically that the traditional plane-wave model is a particular case of the higher-order model, see Section 2.3 for details.

Single-Mode Analysis

In order to address the performance of the HQ tube to suppress higher-order modes, an analysis was performed in which the disturbance is comprised of a single mode. In this analysis, the finite piston sources generate the same single mode as included in the disturbance and the system dimensions are as follows; *h=25.4 cm, S=1.27 cm, L=12.7 cm, ℓ=10.16 cm,* and x_c*=25.0 cm*.

Figure 3.3 depicts this analysis for the first four modes, i.e. *m=0, 1, 2,*and *3*. Each subplot in this Figure contains three graphs. The first is the left and right-hand side of Equation (2.53), the second is the phase difference between the two waves at the second tube-duct interface, and the third is the transmission loss. For example, Figure 3.2a shows that for the *m=0* mode maximum attenuation of *29* and *36 dB* occurring at *1377* and *2747 Hz*, respectively. This subplot also indicates a phase difference of *0.64* and *1.3 rad* at these frequencies. The significance of these phase differences is that for a small area ratio they do not correspond to multiples of λ/2. Similar results are presented for the first three higher-order modes, i.e. *m=1, 2* and *3*, in Figures 3.2(b), 3.2(c) and 3.2(d), respectively. What is obvious is that the frequencies of maximum attenuation are different for each mode and that with increasing modal order these frequencies also increase.

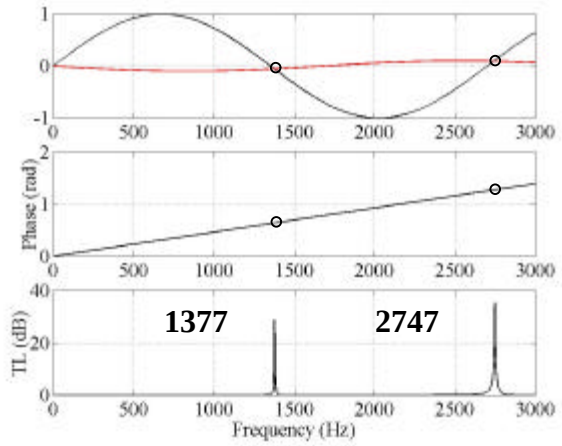

(a) *m=0*

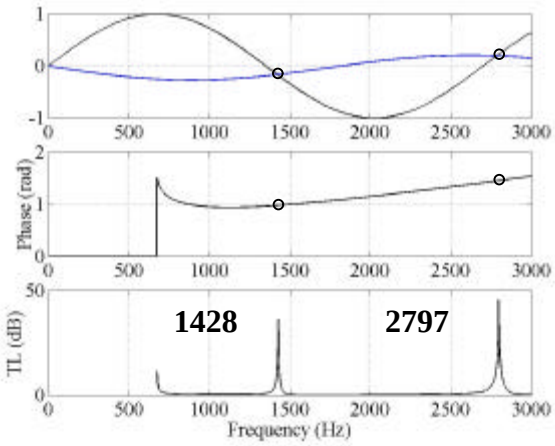

(b) *m=1*

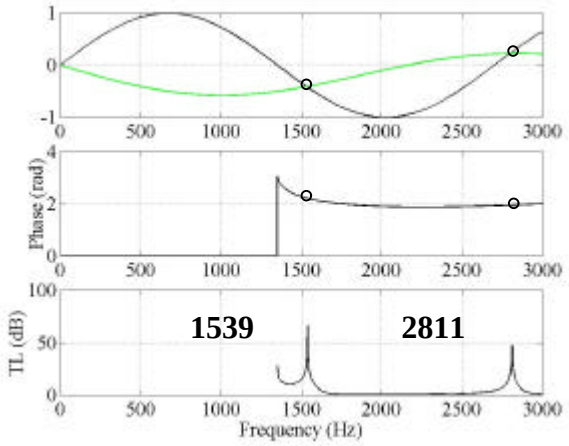

(c) *m=2*

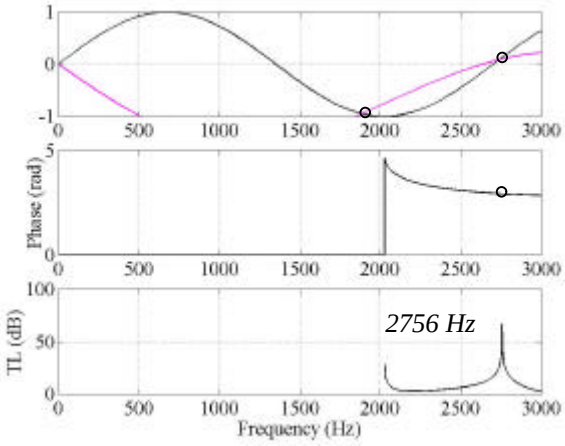

(d) *m=3*

Figure 3.3. Single-mode frequencies of maximum attenuation, phase difference of recombined waves, and transmission loss for modes; (a) *m=0*, (b) *m=1*, (c) *m=2*, and (d) *m=3*

This same type of single-mode analysis can be used to investigate how system geometric parameters influence the frequencies of maximum attenuation. This is presented in Figure 3.4, for several values of the HQ tube cross-sectional area, *S=0.32, 0.64, 1.27, 2.54,* and *5.08cm* and for the first four system modes. These areas correspond to area ratios ranging from *2.5% - 40%*, see Equation (2.50). It should be kept in mind however that in practice implementation of a HQ tube in an engine would be limited to area ratios of *10%* or less. For this reason the baseline system has an area ratio of *10%*.

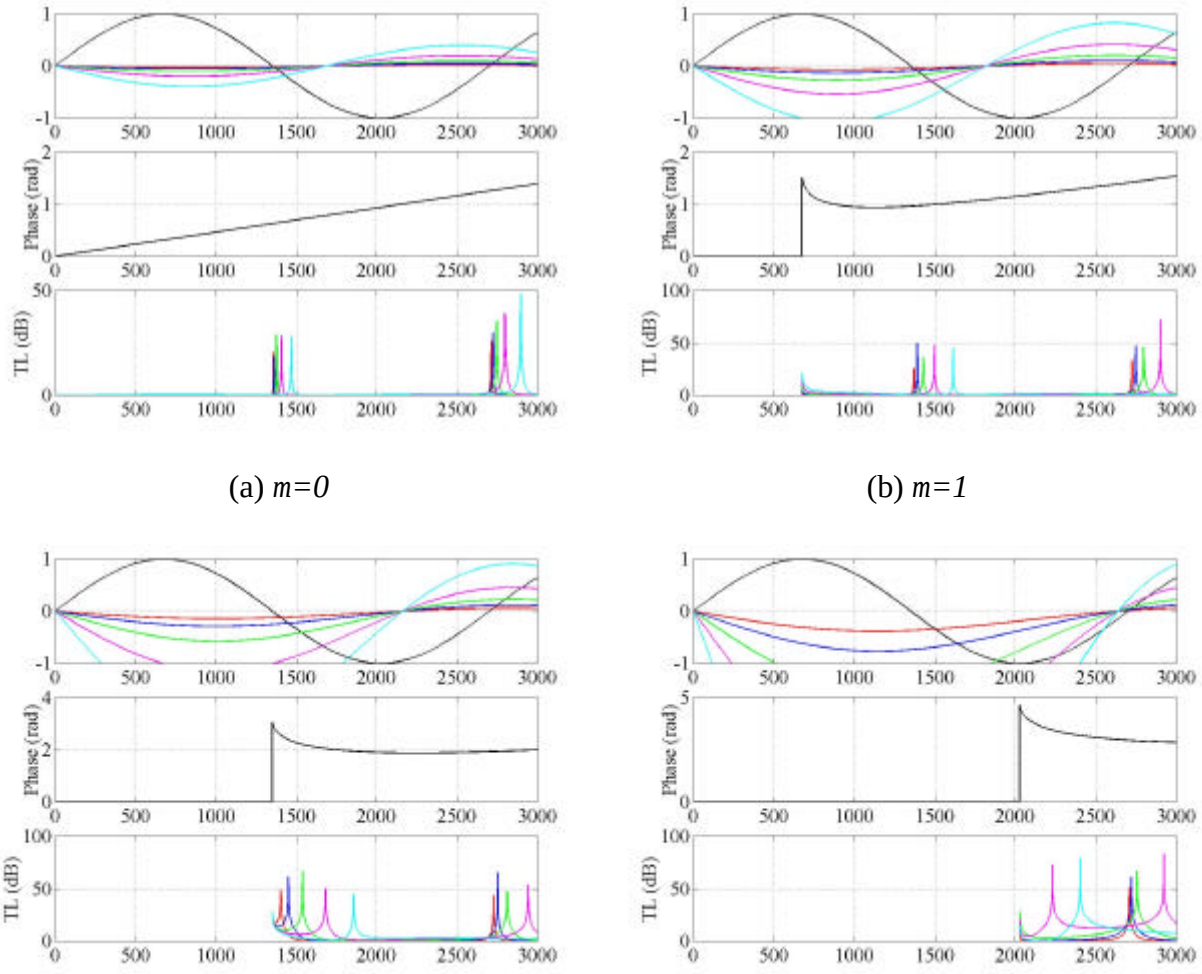

(a) *m=0* (b) *m=1*

(c) *m=2* (d) *m=3*

Figure 3.4. Single-mode analysis of system characteristics with varying HQ tube area, *S=0.32*, *0.64*, *1.27*, *2.54*, and *5.08 cm*, for modes; (a) *m=0*, (b) *m=1*, (c) *m=2*, and (d) *m=3*

In the previous figure, it is interesting to see graphically that as the area of the HQ tube is reduced (*S®0*), the optimum frequencies of attenuation correspond to the natural frequencies of the HQ tube, i.e. *1350* and *2700 Hz*. Also, the highest-order mode presented, the *m=3*, is affected more than the lower modes by the cross-sectional area. Although this type of analysis is shown only for variations in HQ tube cross-sectional area, once the tube length is selected it is useful for investigating any of the other system geometric parameters.

Odd Disturbance Modes

To better understand the performance of the HQ tubes to suppress multiple higher-order modes, a disturbance containing the first two odd modes was next considered. In this analysis, the finite piston sources are capable of generating higher-order modes in the duct, i.e. $N_g=129$. The dimensions of this system remain at $h=25.4$ *cm*, $S=1.27$ *cm*, $L=12.7$ *cm*, $\ell=10.16$ *cm*, and $x_c=25.0$ *cm*. For this system, the cut-on frequencies for the $m=0$, *1*, *2*, *3*, and *4* modes are *0*, *675.2*, *1350*, *2026*, and *2701 Hz*, respectively. The two odd modes, $m=1$ and *3*, are assumed to be present in the incident disturbance field with equal amplitude, $A_{D1}=A_{D3}=1$. Note that due to the symmetric configuration of the HQ tubes, the even modes will not be excited in this system. Thus, the $m=1$ is the only propagating mode in the duct below *2026 Hz* while at higher frequencies both the $m=1$ and *3* are propagating. The resulting transmission loss characteristic are shown in Figure 3.5 for a disturbance comprised of both odd modes, Figure 3.5(a), and for a disturbance comprised of each odd mode individually, Figure 3.5(b).

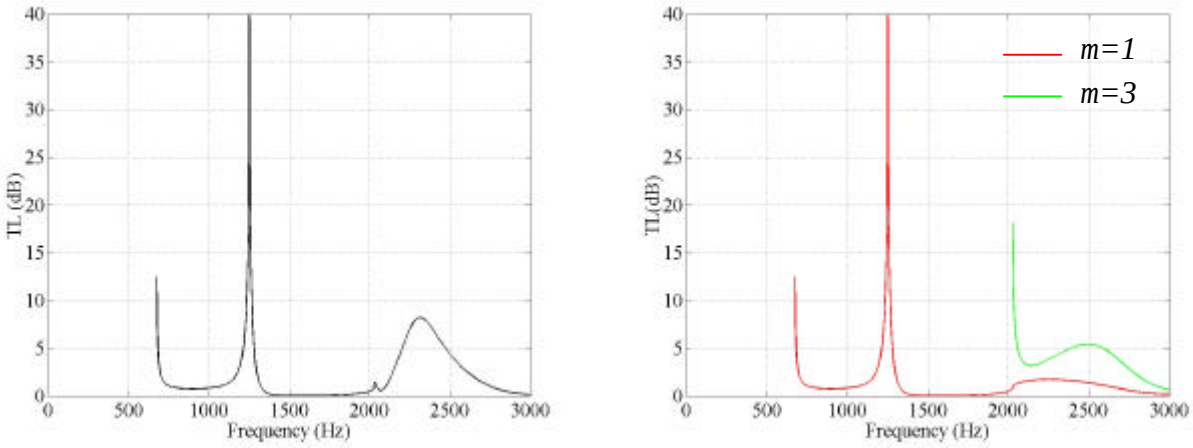

(a) (b)

Figure 3.5. Transmission loss (dB) versus frequency (Hz) for HQ system with disturbance comprised of the odd modes $m=1$ and *3*; (a) together and (b) independently

Substantial attenuation is clearly achieved at *1250 Hz* due to the reflection of the only mode present, i.e. $m=1$ at this frequency. This result is not unexpected since the HQ tubes are very effective at suppressing single modes as in the case of plane-wave mode in Figure 3.2. On the other hand, at *2495 Hz* the transmission loss is *4.5 dB* due to the attenuation of both odd

higher-order modes, i.e. *m=1* and *3*. This is evident by plotting the complex amplitude of the incident, transmitted, and reflected waves for each mode at the frequency of *2495 Hz*. This is shown in Figure 3.6.

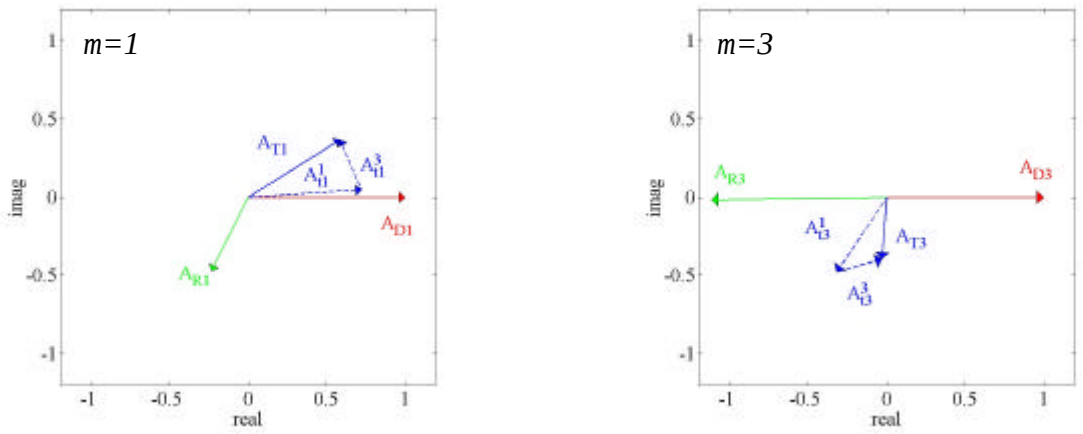

(a) (b)

Figure 3.6. Modal amplitude vectors at *2495 Hz* for disturbance comprised of *m=1* and *3* modes; (a) *m=1* modal amplitudes and (b) *m=3* modal amplitudes

Figure 3.6(a) shows that the *m=1* incident mode, $A_{D1} = 1$, was reflected back with complex amplitude A_{R1}, yielding a net transmitted wave with amplitude A_{T1}. Figure 3.6(b) shows the same analysis for the *m=3* mode. From the modal amplitudes, the sound power reduction of the *m=1* and *3* modes is 3.2 and 8.0 dB, respectively. Thus, these results demonstrate that the HQ tubes are also effective in reducing multiple higher-order modes in a duct. It is also very interesting to note that the amplitude of the reflected *m=3* mode is larger than the amplitude of the incident *m=3* mode, i.e. $A_{R3} > A_{D3}$, see Table 3.1 which lists the power and the amplitude of each of the of the modal components. This clearly implies that some of the acoustic energy from the *m=1* mode has to be spilled over into the *m=3* mode. Thus, the attenuation due to the HQ tubes can not simply be explained as reflection of the mode back to the source.

	Power (dB)		**Magnitude of Modal Amplitude**	
	m=1	***m=3***	***m=1***	***m=3***
Disturbance	81.7	79.5	1.00	1.00
Reflected	76.1	80.5	0.52	1.12
Transmitted	78.5	71.5	0.69	0.40

Table 3.1. Power and amplitudes of modal components at *2495Hz* for odd modes *m=1* and *3*

In order to gain further insight into the noise control mechanisms involved in the suppression of multiple higher-order modes, a modal analysis is carried out where the amplitude of the reflected and transmitted waves are computed for each of the incident modes applied independently. This analysis is presented in Figures 3.7(a) through 3.7(d). For example, Figure 3.7(a) shows the incident *m=1* mode amplitude, $A_{D1} = 1$, and the resulting transmitted, A_{t1}^{1}, and reflected, A_{r1}^{1}, wave amplitudes for mode *m=1*. Note that these amplitudes are different than the ones in Figure 3.6(a) which again indicates that there are interaction effects between the modes. Figure 3.7(b) shows the resulting transmitted, A_{t3}^{1}, and reflected, A_{r3}^{1}, wave amplitudes for mode *m=3* due to the disturbance mode *m=1*. The conclusion of this is that some of the energy from the *m=1* mode is spilled over into the *m=3* mode. Figures 3.7(c) and 3.7(d) show the same analysis for the case of the disturbance consisting of only the *m=3* mode with the same general conclusions. This sort of analysis is valid because the system is linear.

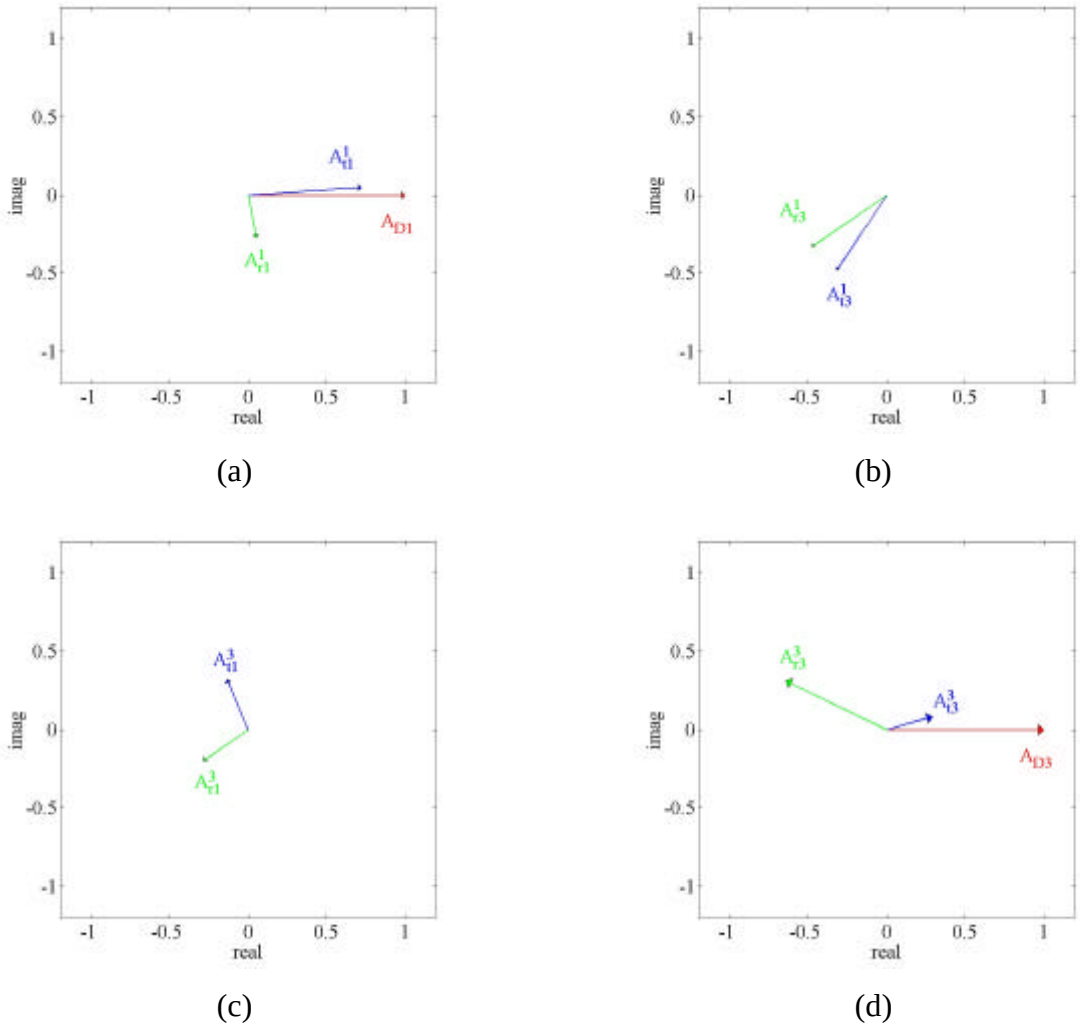

Figure 3.7. Modal amplitude vectors at *2495 Hz*; (a) and (b) disturbance consists of *m=1* mode, (c) and (d) disturbance consists of *m=3* mode only

These plots clearly demonstrate that there are two mechanisms in the reduction of the incident modes. Firstly, the energy in an incident mode is in part reflected back to the source, the same as in the classical plane-wave analysis. Secondly there is some energy spilled from one mode into the other mode. The results in Figure 3.7 also suggest that there is more energy spilled from the low-order mode *m=1* into the higher-order mode *m=3* than vice-versa, i.e. $A^1_{t3} > A^3_{t1}$. Note that the energy spilled into other modes will propagate both upstream and downstream as transmitted and reflected waves, respectively. This is evident in the fact that $A^1_{t3} = A^1_{r3}$ and $A^3_{t1} = A^3_{r1}$. The upstream or transmitted components, A^1_{t3} and A^3_{t1}, will then

contribute to the total transmitted sound power. Thus, the suppression of a particular mode is due to the combination of the spilled-over contributions from the various incident modes. This is demonstrated in Figure 3.6(b) which illustrates the suppression of the *m=3* mode. Using the principle of linear superposition, the resulting transmitted wave of the *m=3* mode, A_{T3}, is due to the vector sum of the spill of the *m=1* mode into the *m=3* mode, A_{t3}^{1}, and the transmitted component due to the same *m=3* mode, A_{t3}^{3}. Thus, the net transmitted wave for the *m=3* mode is the vector sum $\vec{A}_{T3} = \vec{A}_{t3}^{1} + \vec{A}_{t3}^{3}$ which is indicated in dotted lines in Figure 3.6(b). This behavior should be contrasted to the traditional plane-wave analysis of the HQ tube where the only noise reduction mechanism that takes place is reflection of the incident plane-wave.

Even Disturbance Modes

Using the same method to illustrate the dynamics of the odd modes, the even modes for the same system will be described. Again, the system dimensions are *h=25.4 cm, S=1.27 cm, L=12.7 cm, ℓ=10.16 cm,* and x_c*=25.0 cm* resulting in cut-on frequencies for the *m=0, 1, 2, 3,* and *4* modes of *0, 675.2, 1350, 2026,* and *2701 Hz,* respectively. The three even modes, *m=0, 2* and *4*, are assumed to be present in the incident disturbance field with equal amplitude, $A_{D0}=A_{D2}=A_{D4=}1$. Note that due to the symmetric configuration of the HQ tubes, the odd modes will not be excited in this system. Thus, the *m=0* is the only propagating mode in the duct below *1350 Hz*, above *1350 Hz* but below *2701 Hz* both the *m=0* and *2* modes are propagating, and at higher frequencies, those above *2701 Hz*, all of the even modes *m=0, 2* and *4* are propagating. The resulting transmission loss characteristics are shown in Figure 3.8 for both a disturbance comprised of all three even modes, Figure 3.8(a), and for a disturbance comprised of each mode independently, Figure 3.8(b).

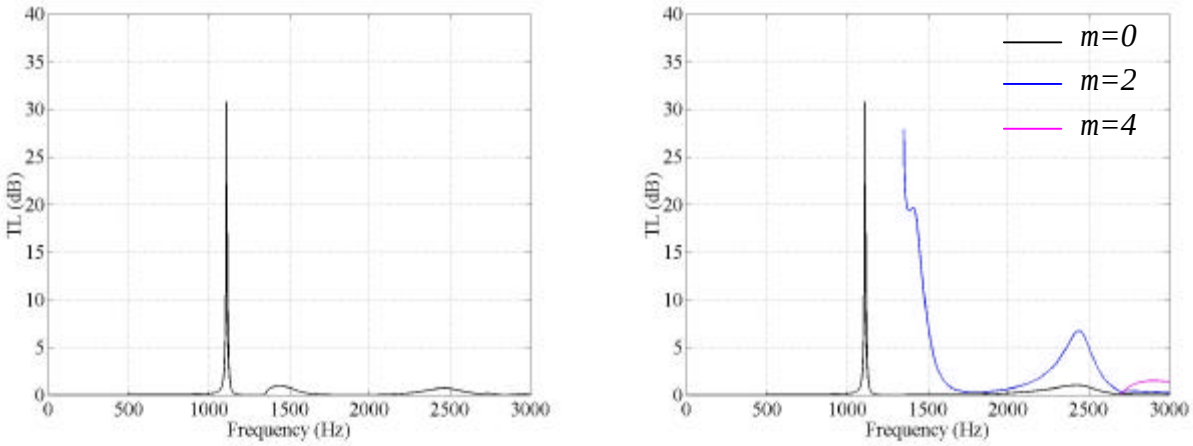

(a) (b)

Figure 3.8. Transmission loss (dB) versus frequency (Hz) for HQ system with disturbance consisting of; (a) all even modes, *m=0, 2* and *4*, and (b) even modes independently

Referring to Figure 3.8(a), which depicts the transmission loss characteristics for a disturbance comprised of all three even modes, substantial attenuation again is clearly achieved at *1111 Hz* due to the reflection of the only mode present, i.e. *m=0*, at this frequency. This result is not unexpected since the HQ tubes are very effective at suppressing single modes. However, what is also apparent is that, unlike the odd modes case, there is not any other substantial attenuation at another frequency. Specifically, at *2495 Hz* there is less than *1 dB* in noise attenuation.

Shown in Figure 3.8(b) are the transmission loss curves for the system with a disturbance comprised of each even mode individually. In this figure, it is clear that there is substantial power attenuation, *5.3 dB*, of the *m=2* mode at *2495 Hz*. To gain further insight into the performance for these modes, further studies are carried out by plotting the complex amplitude of the incident, transmitted, and reflected waves for each mode at the frequency of *2495 Hz*. This analysis is shown in Figure 3.9.

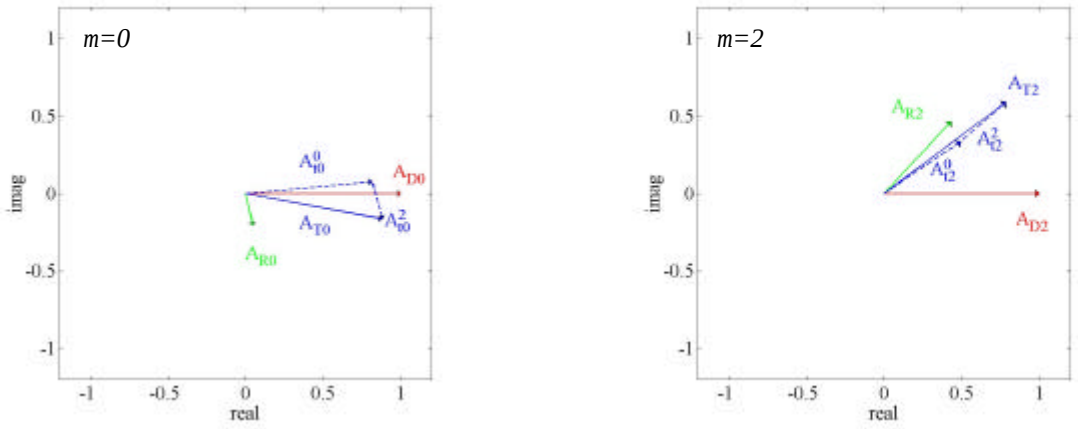

(a) (b)

Figure 3.9. Modal amplitude vectors at *2495 Hz* for disturbance comprised of *m=0*, *2*, and *4* modes; (a) *m=0* modal amplitudes and (b) *m=2* modal amplitudes

Figure 3.9(a) shows for the *m=0* mode that only a small amount of the incident wave, $A_{D0} = 1$, was reflected back with complex amplitude A_{R0}, yielding a net transmitted wave with amplitude A_{T0}. Figure 3.9(b) shows the same analysis for the *m=2* mode, where again most of the incident wave was transmitted with complex amplitude A_{T2}. From the modal amplitudes, the sound power reduction of the *m=0* and *2* modes is *0.96* and *0.16 dB*, respectively. This information is summarized in Table 3.2 which lists the power and the amplitude of each of the of the modal components. Thus, these results again demonstrate, that for a disturbance comprised of all of the even modes, there is negligible reduction at *2495 Hz*. Note that the *m=4* mode has a cut-on frequency of *2701 Hz* and is therefor not present at this frequency.

	Power (dB)		**Magnitude of Modal Amplitude**	
	m=0	***m=2***	***m=0***	***m=2***
Disturbance	84.9	81.1	1.00	1.00
Reflected	71.3	77.1	0.21	0.63
Transmitted	83.9	80.9	0.90	0.98

Table 3.2. Power and amplitudes of modal components at *2495Hz* for even modes *m=0* and *2*

In order to again gain further insight into the noise control mechanisms involved, a modal analysis is carried out where the amplitude of the reflected and transmitted waves are computed for each of the incident modes independently. This analysis is presented in Figures 3.10(a) through 3.10(d). For example, Figure 3.10(a) shows the incident *m=0* mode amplitude, $A_{D0} = 1$, and the resulting transmitted, A_{t0}^{0}, and reflected, A_{r0}^{0}, wave amplitudes for mode *m=0*, while Figure 3.10(b) shows the resulting transmitted, A_{t2}^{0}, and reflected, A_{r2}^{0}, wave amplitudes for mode *m=2* due to the disturbance mode *m=0*. Figures 3.10(c) and 3.10(d) show the same analysis for the case of the disturbance consisting of only the *m=2* mode.

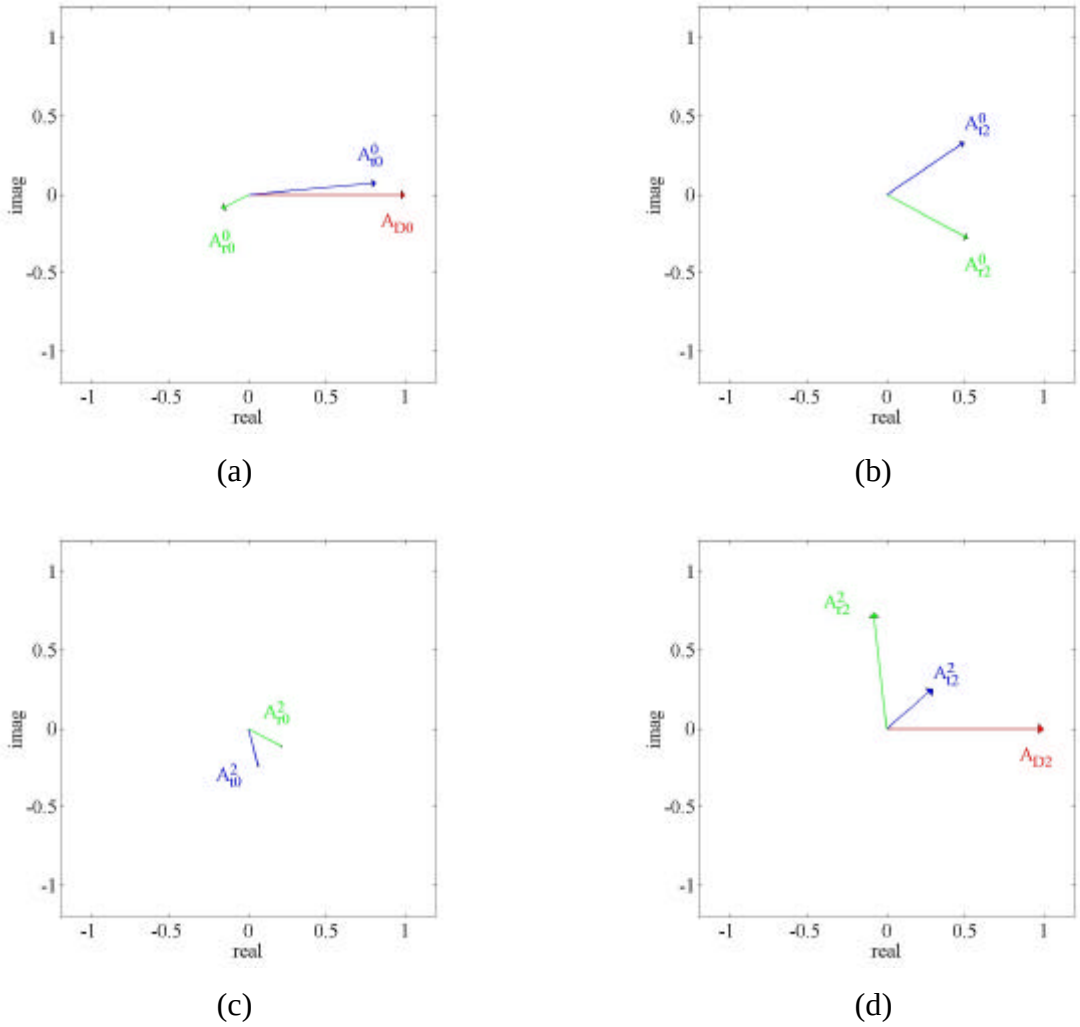

Figure 3.10. Modal amplitude vectors at *2495 Hz*; (a) and (b) disturbance consists of *m=0* mode; (c) and (d) disturbance consists of *m=2* mode only

Considering the case in which the disturbance is comprised of the *m=0* mode only, Figure 3.10(a)-(b), it is clear that most of the incident wave energy, A_{D0}, is transmitted in the *m=0* component of the transmitted wave, termed A_{t0}^{0}. However, there has been a small amount of energy reflected in the *m=0* component of the reflected wave, A_{R0}^{0}, and some spill of energy into both the transmitted and reflected components of the *m=2* mode, A_{t2}^{0} and A_{r0}^{0} respectively. This behavior illustrates what is already known about the sound attenuation at this frequency from Figure 3.8(b). Namely, that for a disturbance comprised of the *m=0* mode only, there is very little transmission loss at *2495 Hz*.

Figure 3.10(c)-(d) depict the case in which the disturbance is comprised of the *m=2* mode only, A_{D2}. From these plots, it is evident that a small portion of the incident wave energy has spilled into the transmitted and reflected components of the *m=0* mode, A_{t0}^{2} and A_{r0}^{2} respectively. In addition, it can be seen that most of the incident wave energy is reflected in the *m=2* component of the reflected wave, A_{r2}^{2}. This explains the reason there is sound attenuation at 2495 Hz for a disturbance comprised of only the *m=2* mode, as seen in Figure 3.8(b).

Like the odd modes case, these plots show that there are two mechanisms involved in the modal reconstruction of the incident modes. First, the incident wave energy is in part reflected back to the source, and second there is some energy spilled into the other higher-order modes. This spilled energy will propagate both upstream and downstream as transmitted and reflected waves respectively. The upstream component contributes to the total transmitted sound power. These results also suggest that there is more energy spilled from the low-order mode *m=0* into the higher-order mode *m=2* than vice-versa, i.e. $A_{t2}^{0} > A_{t0}^{2}$.

As mentioned before, the suppression of a particular mode is due to the combination of the spilled-over contributions from the various incident modes. This is demonstrated in Figure 3.9(b) as vector sums indicated as dashed lines. For example, the resulting transmitted *m=2* mode, A_{T2} is due to the vector sum of the spill of the *m=0* mode into the *m=2* mode, A_{t2}^{0}, and the

transmitted component due to the same *m=2* mode, A_{t2}^{2}, i.e. $\vec{A}_{T2} = \vec{A}_{t2}^{0} + \vec{A}_{t2}^{2}$. However, in this case the two components $\vec{A}_{t2}^{0}$ and $\vec{A}_{t2}^{2}$ are nearly in phase and their contributions do not cancel each other, as was the case for the odd mode disturbances in Figure 3.6. Further investigation in later sections will show that various system parameters affect the spill-over / addition behavior.

All Disturbance Modes

In the two previous sections, the suppression of the even and odd disturbance modes has been studied in detail, but independently. For the sake of completeness, the analysis of the HQ tube system is extended to include all of the even and odd cut-on disturbance modes in the frequency range of interest. The same system geometric parameters are used with *h=25.4 cm, S=1.27 cm, L=12.7 cm, ℓ=10.16 cm,* and x_c*=25.0 cm.* Resulting in cut-on frequencies for the *m=0, 1, 2, 3,* and *4* modes of *0, 675.2, 1350, 2026,* and *2701 Hz,* respectively. The first five modes, *m=0, 1, 2, 3,* and *4,* are assumed to be present in the incident disturbance field with equal amplitude, $A_{D0}=A_{D1}=A_{D2}=A_{D3}=A_{D4}=1$. The resulting transmission loss characteristic is shown in Figure 3.11.

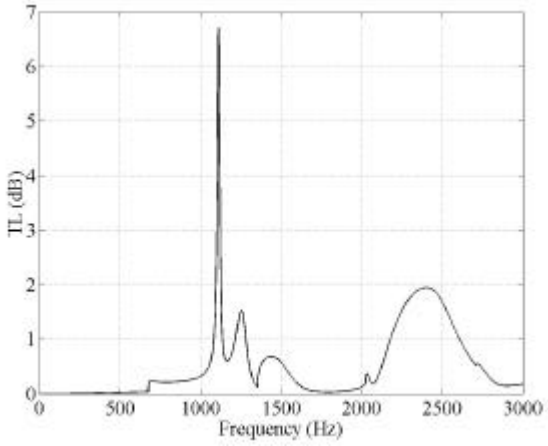

Figure 3.11. Transmission loss (dB) versus frequency (Hz) for HQ system comprised of all six cut-off disturbance modes *m=0, 1, 2, 3,* and *4*

At *1111 Hz*, the transmission loss is *6.7 dB* due to the attenuation of both the plane wave, *m=0*, and the first higher-order, *m=1*, modes. Centered around *2400 Hz*, is a band of attenuation with a peak of *2.0 dB*. At this frequency, this reduction is due to the attenuation of the first four modes, *m=0, 1, 2,*and *3*. This band of attenuation is studied by plotting the complex amplitudes of the transmitted waves for each mode for the frequency of *2400 Hz*, this is shown in Figure 3.12.

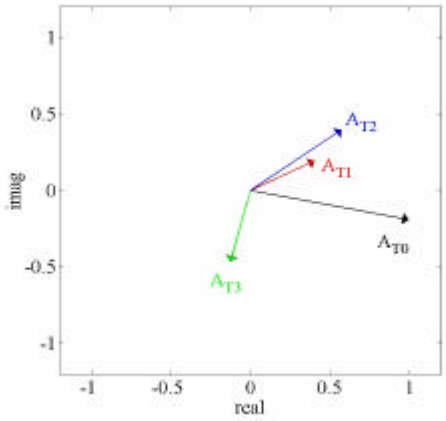

Figure 3.12. Transmitted modal amplitude vectors at *2400 Hz* for disturbance comprised of *m=0, 1, 2, 3*, and *4* modes

In this figure, the complex modal amplitudes, in black, red, blue, and green colors are used to represent the *m=0*, *1*, *2*, and *3* modes respectively and should not be confused with the color scheme used in previous sections to represent incident, transmitted, and reflected wave amplitudes. It is clear that there is a reduction in the magnitude of the modal amplitudes, see Table 3.3. This reduction in magnitude leads to the attenuation of power. In addition, it can be seen that there is a change in phase of the complex amplitudes.

	Power (dB)				**Magnitude of Modal Amplitude**			
	m=0	***m=1***	***m=2***	***m=3***	***m=0***	***m=1***	***m=2***	***m=3***
Disturbance	84.9	81.7	81.1	79.5	1.00	1.00	1.00	1.00
Reflected	71.3	76.1	77.1	80.5	0.21	0.61	0.60	1.25
Transmitted	83.9	78.5	80.9	71.5	1.01	0.45	0.70	0.48

Table 3.3. Power and amplitudes of modal components at *2400Hz* for modes *m=0, 1, 2,* and *3*

It is important to study how the array of HQ tubes produces this reduction in the disturbance modal amplitudes. In order to accomplish this, a modal analysis is performed in which the transmitted modes are computed for each of the incident modes independently. This analysis is presented in Figures 3.13(a) through 3.13(d). For example, Figure 3.13(a) shows the incident *m=0* mode (black solid line) amplitude, $A_{D0} = 1$, and the resulting transmitted wave amplitudes, A_{t0}^{0} and, A_{t2}^{0}, for mode *m=0* and *m=2*, while Figure 3.13(b) shows the resulting transmitted wave amplitudes, A_{t0}^{2} and A_{t2}^{2}, for mode *m=0* and *m=2* due to the disturbance mode *m=2* (blue solid line). Figures 3.13(c) and 3.13(d) show the same analysis for the case of the disturbance consisting of the *m=1* and *m=3* mode respectively. It should be noted that at this frequency the *m=4* mode is not cut-on.

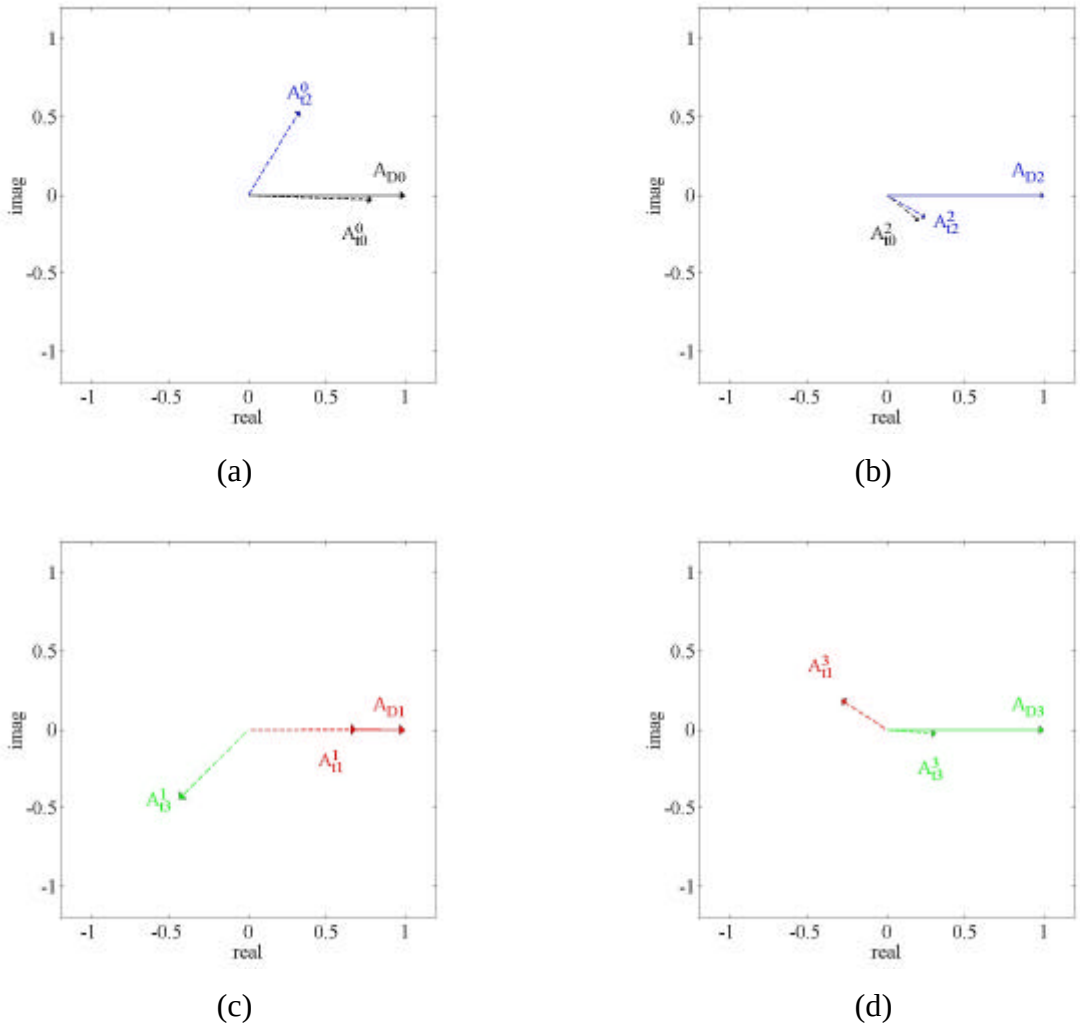

Figure 3.13. Transmitted modal amplitude vectors at *2400 Hz* with disturbance consisting of mode; (a) *m=0*, (b) *m=2*, (c) *m=1*, and (d) *m=3*

Again, from these plots it can be seen that there are two mechanisms in the reduction of the incident modes. A part of the incident energy is reflected back to the source, and secondly there is some energy spilled into the other higher-order modes. The suppression of a mode is due to the combination of the spilled-over contributions from the various incident modes. This is demonstrated in Figure 3.14 which illustrates the suppression of the *m=3* disturbance mode, A_{T3}. The resulting transmitted wave of the *m=3* mode is due to the vector sum of the spill of the *m=1* mode into the *m=3* mode, A_{t3}^{1}, and the transmitted component due to the same *m=3* mode, A_{t3}^{3}.

Thus, the net transmitted wave for the *m=3* mode is $A_{T3} = A_{t3}^{1} + A_{t3}^{3}$ which is indicated as a vector sum in a solid line in Figure 3.14.

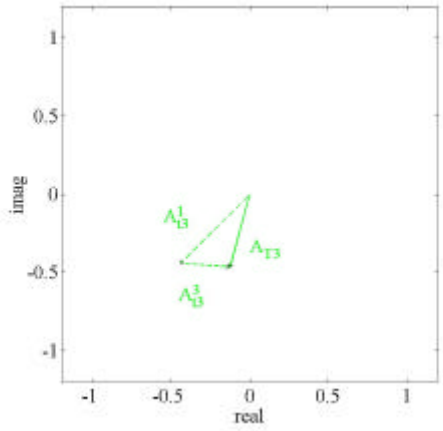

Figure 3.14. Modal suppression of transmitted mode *m=3* at *2400 Hz*, disturbance consists of *m=0, 1, 2, 3,* and *4* modes

3.2 Parametric Studies

This section continues to describe the noise reduction mechanisms involved in the attenuation of higher-order mode acoustic disturbances. This is accomplished by examining the system transmission loss characteristics by changing geometric parameters such as tube length, distance between interfaces, cross-sectional area, axial position, and the number of tube arrays. The number of modes included in the Green's functions was *130*, including the plane-wave mode, or N_g*=129*.

Tube Geometric Parameters: Axial Location, Length, Interface Distance, and Area

The attenuation of higher-order mode acoustic disturbances has been attributed to the reflection of energy, the spill of energy between modes, and the reconstruction of components in each mode. Since the phase of each mode changes as it propagates down the duct, system geometric parameters exist which influence the modally restructured magnitudes and phases to optimally recombine, resulting in the minimum overall transmitted amplitude. Such influential

system characteristics are tube axial position (x_c), length (L), distance between interfaces (ℓ), and area (S).

Numerical results were computed using the two symmetrically located HQ tubes as shown in Figure 2.3. The baseline dimensions of this system are $h=25.4$ *cm*, $S= 1.27$ *cm*, $L=12.7$ *cm*, $\ell=10.16$ *cm*, and $x_c=25.0$ *cm*. Resulting in cut-on frequencies for the $m=0$, *1*, *2*, *3*, and *4* modes of *0*, *675.2*, *1350*, *2026*, and *2701 Hz*, respectively. The first five modes, $m=0$, *1*, *2*, *3*, and *4*, are assumed to be present in the incident disturbance field with equal amplitude, $A_{D0}=A_{D1}= A_{D2}= A_{D3}= A_{D4}=1$. The number of modes included in the Green's functions were $N_g=129$.

Effect of Axial Position

In Figure 3.15(a), the transmission loss characteristic is shown versus the axial position x_c of the HQ tube for a frequency of *2400 Hz*. The transmission loss for a range of frequencies, *0-3000 Hz* is presented in Figure 3.15(b). Clearly, the distance x_c has a significant influence on the attenuation of specific modes. For instance, there exists a location $x_{c,opt}$ which is optimum for the attenuation of all five of the disturbance modes. In addition, the optimal location repeats periodically down the duct. Figure 3.15 (b) shows that the frequency of maximum attenuation is insensitive of the axial position of the HQ tubes.

The reason for having an optimal axial location for the HQ tubes is that the relative phase between the modes changes as they propagate along the duct because of their different axial wavenumbers. This implies that at some position along the duct the phase of the modes is such that leads to the best recombination of the spill of energy between the modes and minimum net transmitted power. Again this behavior should be contrasted to the case of controlling a single mode where the reduction is independent of the axial position of the HQ tubes.

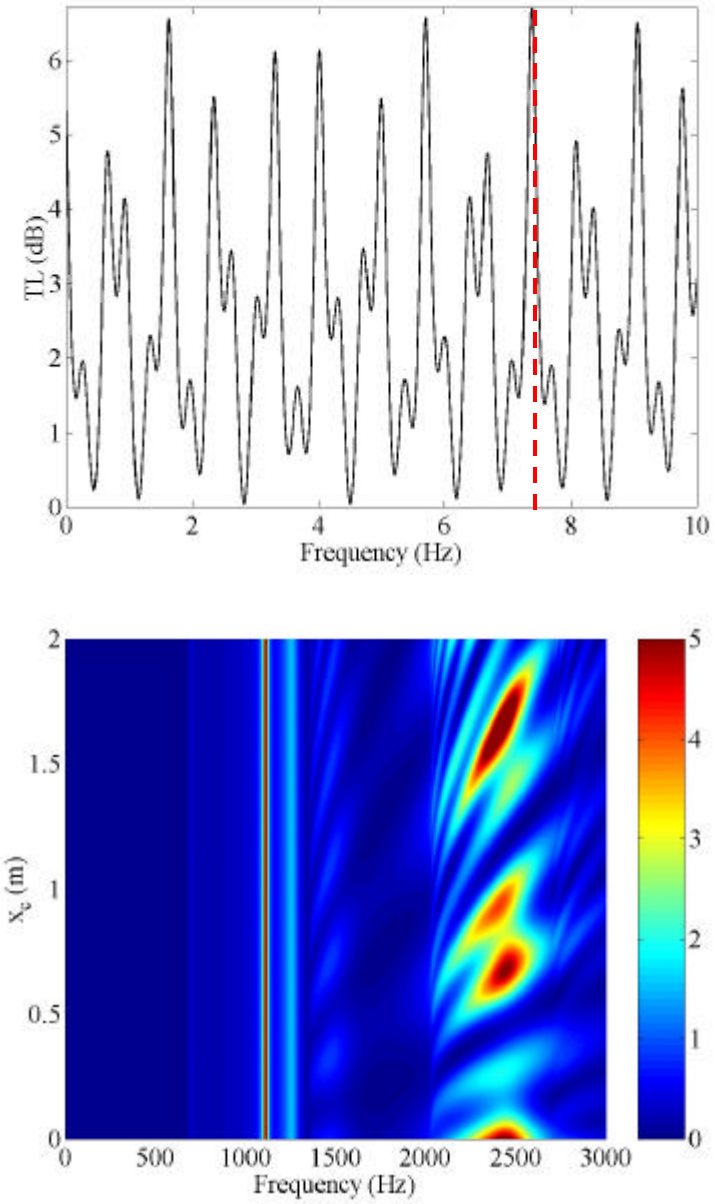

(a)

(b)

Figure 3.15. Transmission loss (dB) versus tube axial location, x_c *(m)*, with disturbance comprised of *m=0, 1, 2, 3,* and *4* modes at (a) *2400 Hz* and (b) *0-3000 Hz*

Figure 3.16 shows the modal components of the transmitted wave amplitudes at *2400 Hz* for a unit modal amplitude of the incident modes, *m=0, 1, 2, 3,* and *4*, and for the range of values of the tube axial location, i.e. x_c*=0 to 0.29 m*. The range of modal amplitudes corresponding to the range of x_c values are indicated by the curve connecting the two vectors associated to the

lower and upper values of the range. This figure shows that the magnitude and phase of the modes are greatly affected by the tube axial location.

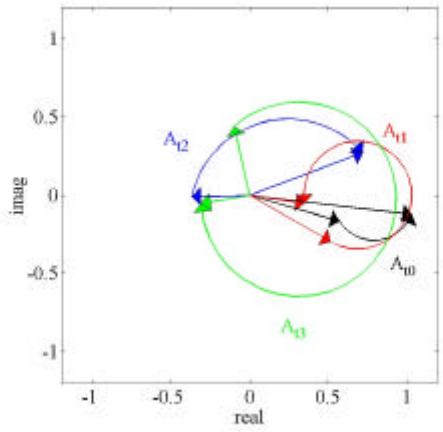

Figure 3.16. Transmitted modal amplitude vectors at *2400 Hz* for x_c*=0 - 0.29 m* and disturbance comprised of *m=0, 1, 2, 3,* and *4* modes

Effect of Tube Length

The influence of the length of the HQ tube, *L*, for all five disturbance modes, is shown in Figure 3.17 for a frequency of *2400 Hz* in Figure 3.17(a) and for the range of frequencies *0-3000 Hz* in Figure 3.17(b). These results show that the HQ tube length is also a very important parameter on the attenuation of multiple higher-order modes. In addition, this attenuation repeats periodically, with a period of *0.143 m*. It is interesting to note that considering this periodicity in space as a wavelength, it corresponds to a frequency of approximately *2400 Hz*. This result is quite logical because the attenuation occurs near the HQ tube resonance frequencies and a change in the length of the tube results in a shift of the resonance frequencies. For example, a tube length of *L=0.13 m* results in the second tube resonance to be near *2400 Hz* (*kL=2p*) and thus this resonance is responsible for the sound attenuation. By changing the tube length to *L+D* where *D=2p/k*, the fourth resonance is now near *2400 Hz* and thus is responsible for the attenuation. Within the range of tube lengths studied, maximum attenuation of approximately *2.0 dB* is achieved with a tube length of *0.1284 m* at *2400 Hz*. Figure 3.17(b)

shows that changing the tube length results in a change in the frequency of maximum attenuation. It is clear to identify the bands of attenuation for the 1st, 2nd, etc., tube resonances.

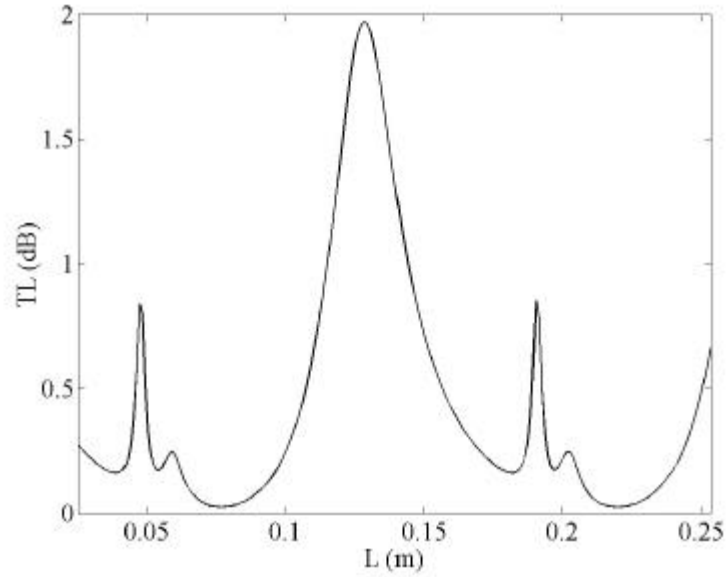

(a)

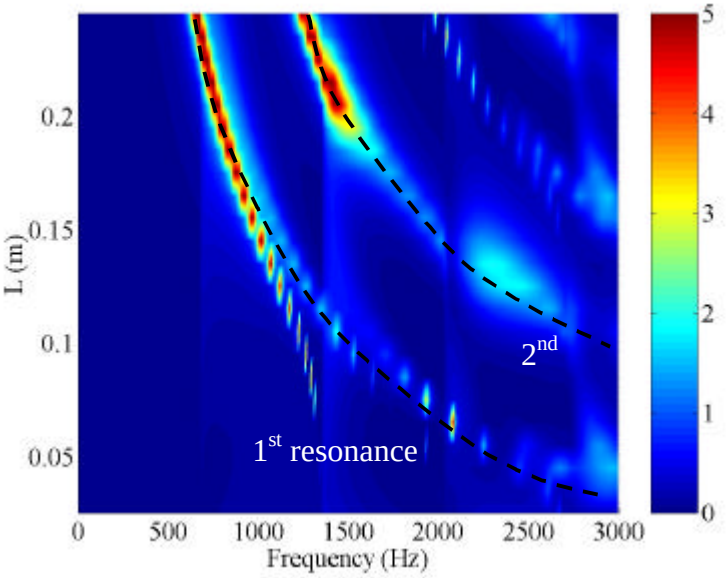

(b)

Figure 3.17. Transmission loss (dB) versus tube length, *L (m)*, with disturbance comprised of *m=0, 1, 2, 3,* and *4* modes at (a) *2400 Hz* and (b) *0-3000 Hz*

Figure 3.18 shows the modal breakdown analysis at *2400 Hz* for a unit modal amplitude of the incident modes and for a range of values of the tube length, i.e. *L=0.1054 – 0.1754 m.*

This figure shows that the magnitude and phase of the modes created by the spill of energy mechanism is greatly affected by the tube length.

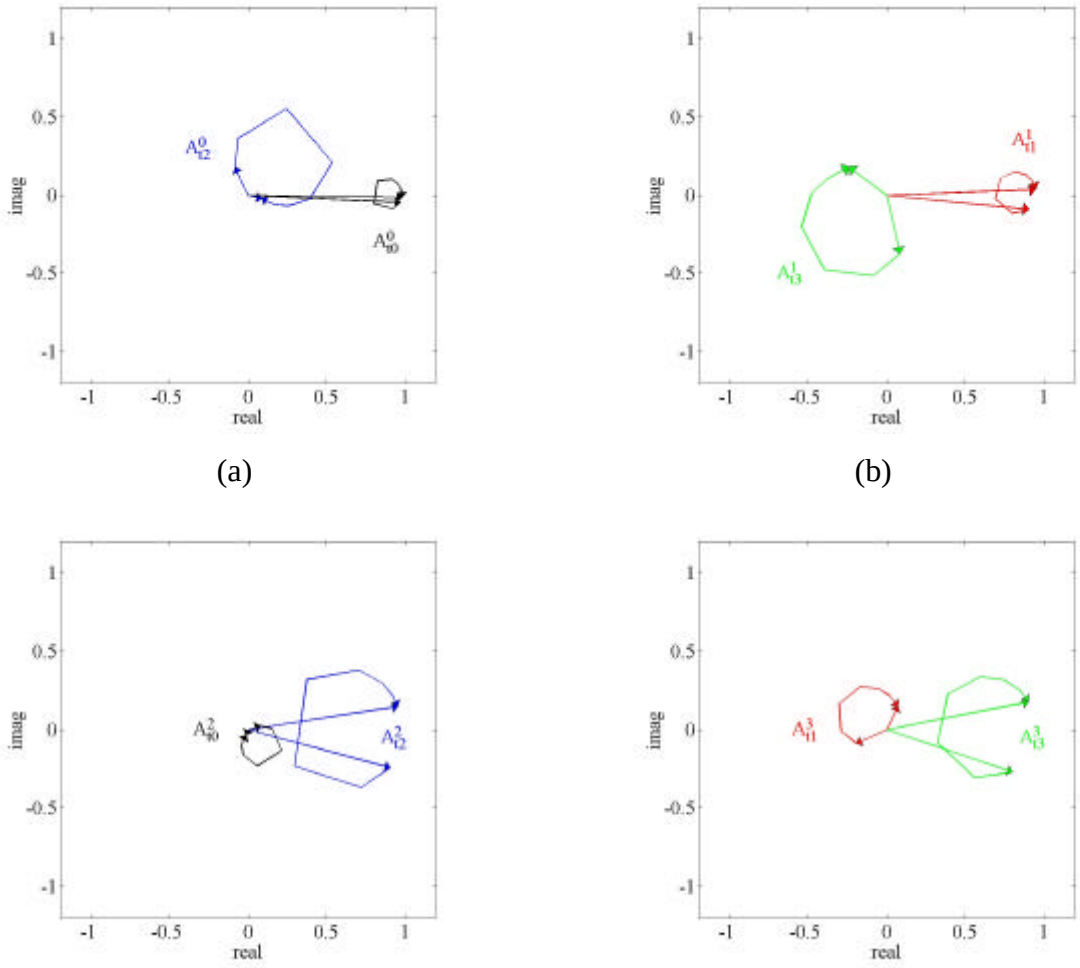

Figure 3.18. Transmitted modal amplitude vectors at *2400 Hz* for *L=0.1054 – 0.1754 m* and disturbance consisting of modes; (a) *m=0*, (b) *m=1*, (c) *m=2*, and (d) *m=3*

Effect of Interface Distance

The influence of the interface distance of the HQ tube, ℓ, for the disturbance comprised of *m=0, 1, 2, 3,* and *4* modes, is shown in Figure 3.19 for a frequency of *2400 Hz* in Figure 3.19(a) and for the range of frequencies *0-3000 Hz* in Figure 3.19(b). The HQ tube interface distance, constrained by the system geometry as $2S < \ell > L$, also influences the attenuation of higher-order

modes. Within the range of tube interface lengths studied, maximum attenuation of approximately *2.1 dB* is achieved with a tube length of *0.0874 m* at *2400 Hz*. Figure 3.18(b) shows that the frequency of maximum attenuation is insensitive of the interface distance of the HQ tubes.

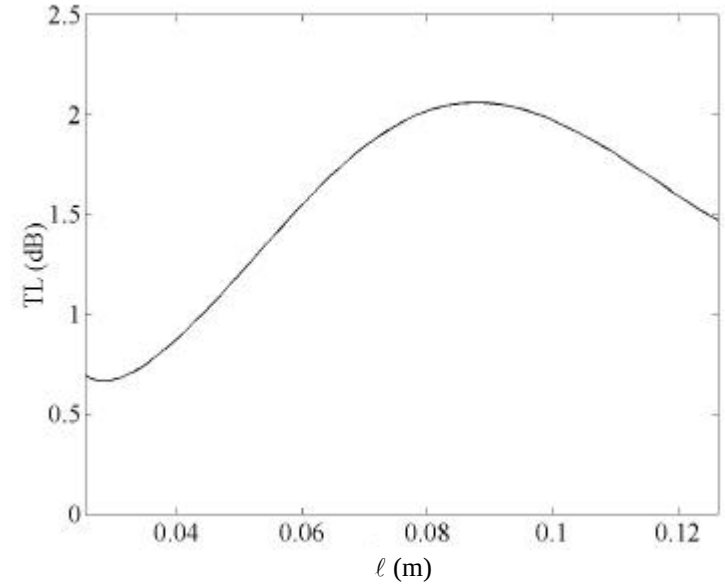

(a)

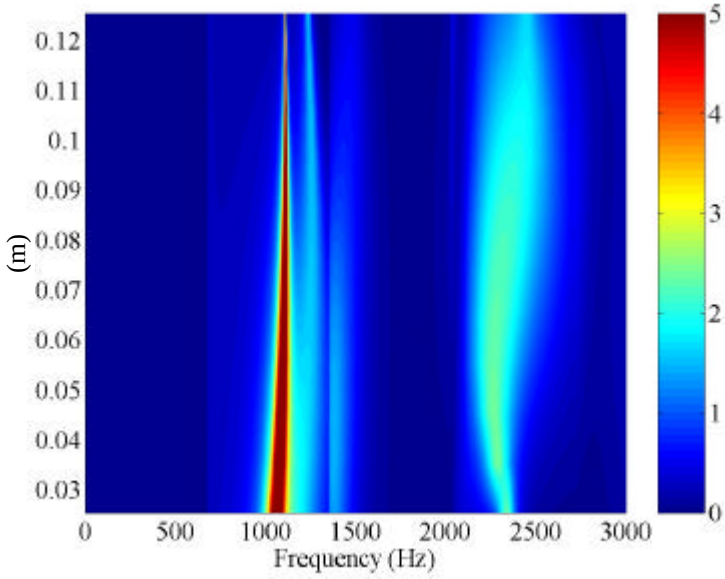

(b)

Figure 3.19. Transmission loss (dB) versus interface distance, *ℓ (m)*, with disturbance comprised of *m=0, 1, 2, 3,* and *4* modes at (a) *2400 Hz* and (b) *0-3000 Hz*

Figure 3.20 shows the modal breakdown analysis at *2400 Hz* for a unit modal amplitude of the incident modes and for a range of values of the tube interface distance, i.e. ℓ*=0.0254 – 0.1254 m*. Again, this type of analysis, shows that the magnitude and phase of the modes created by the spill of energy mechanism is greatly affected by the tube interface distance.

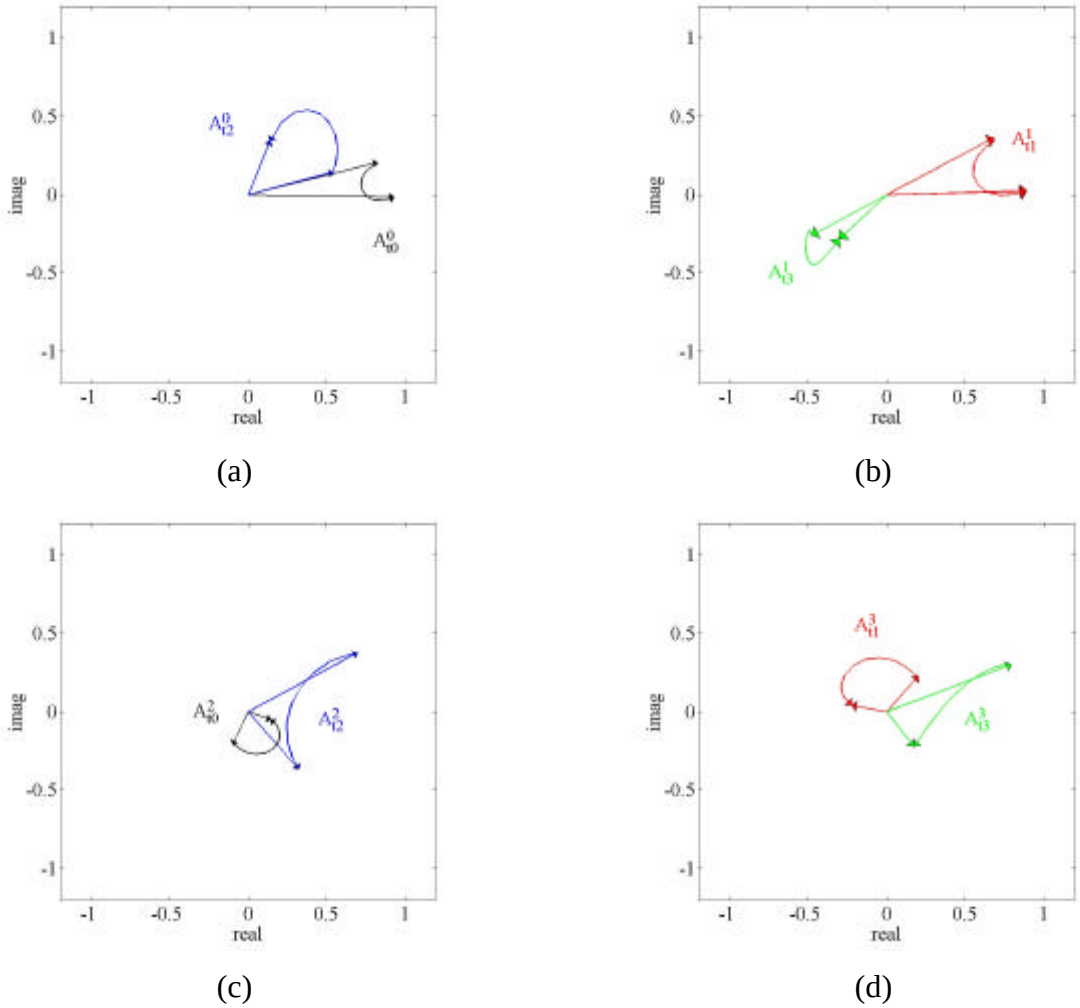

Figure 3.20. Transmitted modal amplitude vectors at *2400 Hz* for ℓ*=0.0254 – 0.1254 m* and disturbance consisting of modes; (a) *m=0*, (b) *m=1*, (c) *m=2*, and (d) *m=3*

Effect of Tube Area

The last parameter, for the single-array HQ tube system, to be studied is the cross-sectional area of the side-tubes, *S*, for the disturbance comprised of *m=0, 1, 2, 3,* and *4* modes. This analysis is shown as a function of area ratio (*AR)*, where *AR=2S/h*, in Figure 3.21 for a

frequency of *2400 Hz* in Figure 3.21(a) and for the range of frequencies *0-3000 Hz* in Figure 3.21(b). Within the range of tube cross-sectional areas studied, maximum attenuation of approximately *2.0 dB* is achieved with an *AR* of *11.8%* at *2400 Hz*. It should be kept in mind, that in the modeling of the side-tube dynamics, the pressure distribution within the tubes was assumed to consist of planes waves only. This method is therefore limited to frequencies well below the first cut-off frequency of the transverse modes in the side-tubes, $c/2S$.

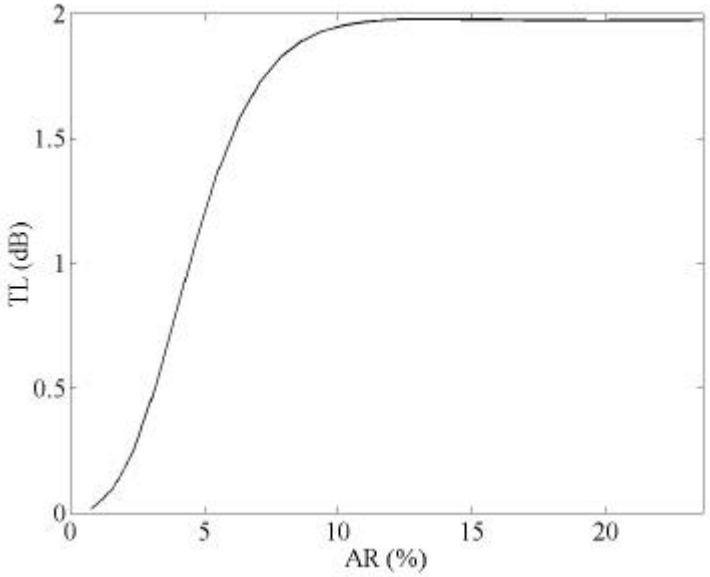

(a)

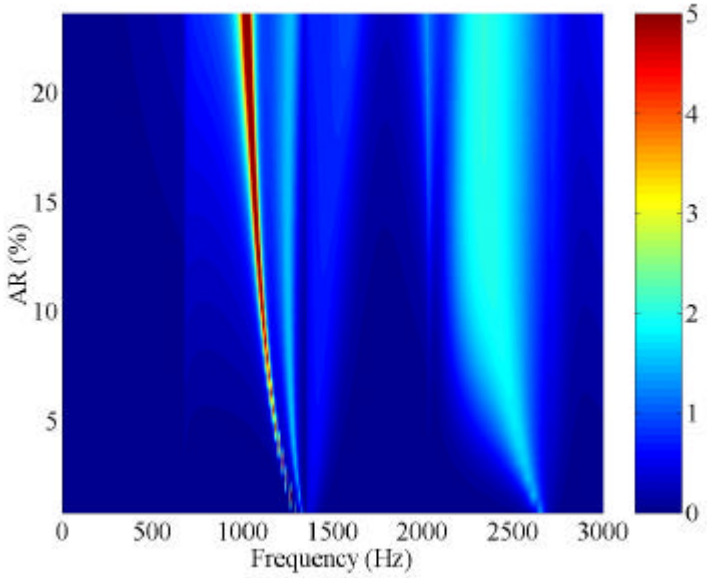

(b)

Figure 3.21. Transmission loss (dB) versus tube area ratio, *AR (%)*, with disturbance comprised of *m=0, 1, 2, 3,* and *4* modes at (a) *2400 Hz* and (b) *0-3000 Hz*

Figure 3.22 shows the modal breakdown analysis at *2400 Hz* for a unit modal amplitude of the incident modes and for a range of values of the tube cross-sectional area, i.e. *S=0.001 – 0.011 m*. Again, this figure shows that the magnitude and phase of the modes created by the spill of energy mechanism is greatly affected by the tube cross-sectional area.

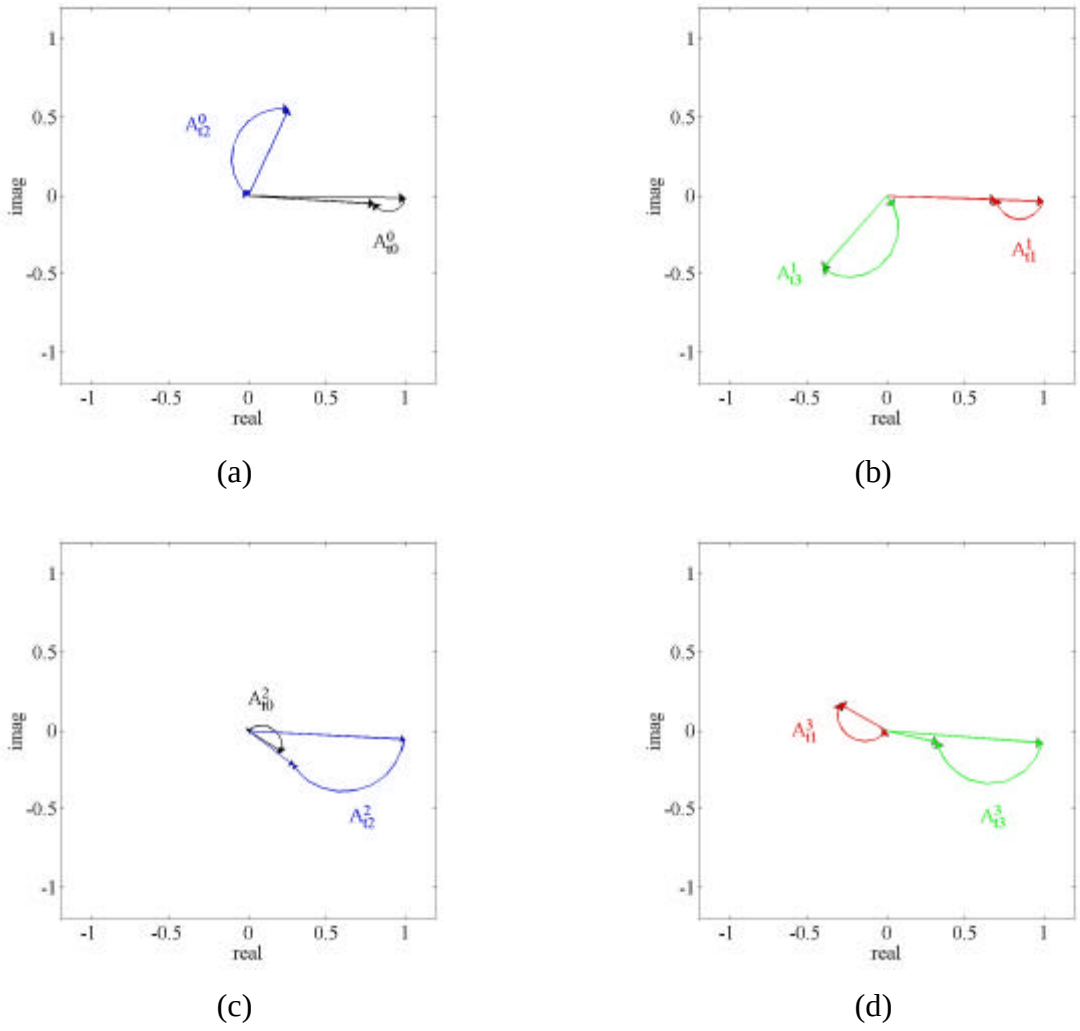

Figure 3.22. Transmitted modal amplitude vectors at *2400 Hz* for *S=0.001 – 0.011 m* and disturbance consisting of modes; (a) *m=0*, (b) *m=1*, (c) *m=2*, and (d) *m=3*

3.3 Tubes in Series

Now that the basic attenuation characteristics and behaviors, for a single-array HQ tube system, have been studied, it is of interest to extend this analysis to include two HQ tube arrays.

Specifically, it is of primary concern to learn whether or not there are attenuation benefits with the addition of a second array of tubes. In general, the addition of a second tube array increases the complexity of the system. It then becomes more difficult to choose system geometric parameters to optimize specific sound attenuation behaviors. In this case, it is assumed that the second array of tubes has the same cross-sectional area, tube length, and interface distance as the first array. There is then only the separation distance, x_{c2}, between the two arrays that is optimized.

To explore this, numerical results were computed using the two symmetrically located HQ tubes in series, as shown in Figure 2.9. The dimensions of this system are $h=25.4$ *cm*, $S=S_2=1.27$ *cm*, $L=L_2=12.7$ *cm*, $\ell=\ell_2=10.16$ *cm*, $x_c=25.0$ *cm*, and $x_{c2}=6.54$ *cm*. Resulting in cut-on frequencies for the $m=0, 1, 2, 3$, and *4* modes of *0, 675.2, 1350, 2026,* and *2701 Hz*, respectively. The first five modes, $m=0, 1, 2, 3$, and *4*, are assumed to be present in the incident disturbance field with equal amplitude, $A_{D0}=A_{D1}=A_{D2}=A_{D3}=A_{D4}=1$. The number of modes included in the Green's functions were $N_g=129$. Figure 3.23 shows a transmission loss comparison between a system comprised of only a single array and one comprised of two HQ tube arrays.

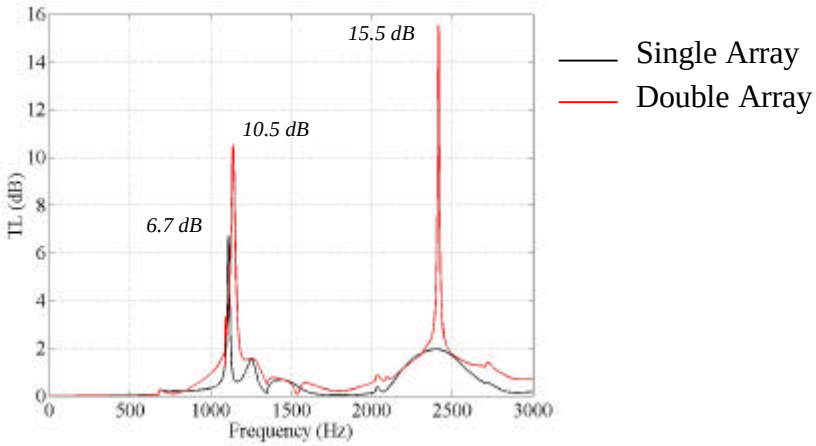

Figure 3.23. Transmission loss (dB) versus frequency (Hz) for both single and double tube-array systems with disturbance comprised of $m=0, 1, 2, 3$, and *4* modes and $x_{c2}=0.0654$ *m*

In the single array system, there is attenuation of *6.7 dB* at *1111 Hz*. In the double array system, the peak attenuation has shifted to *1140 Hz* and increased to *10.5 dB*. In addition, in

both systems, there is a band of attenuation centered on approximately *2400 Hz*. In the single array system, this band has a peak transmission loss of *2.0 dB* where as in the double array system there is *15.5 dB* of noise reduction at *2413 Hz*. The reduction at this frequency, is further studied by computing the complex amplitudes of the transmitted waves for each mode, as a function of the separation distance, x_{c2}. The results are shown below in Figure 3.24. This figure shows that the magnitude and phase of the modes are greatly affected by the separation distance of the two HQ tube arrays. Most importantly, these results show that adding more arrays of HQ tubes can lead to significant improvement of the attenuation of multiple higher-order modes.

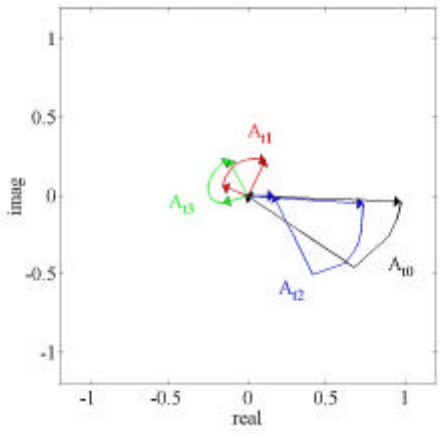

Figure 3.24. Transmitted modal amplitude vectors at *2413 Hz* for double array HQ system with disturbance comprised of *m=0, 1, 2, 3,* and *4* modes and x_{c2}*=0.0254 - 0.0654 m*

Chapter 4 – Conclusions

4.1 Summary

Although the concept of a HQ tube was envisioned by Herschel back in the early 19th century [8], all of the analytical modeling concepts to date, have been limited to one-dimensional sound fields [8-16]. In this thesis, the main goal was to present an analytical modeling technique which would model the effects of Herschel-Quincke (HQ) tubes in the presence of multiple higher-order modes in a two-dimensional duct. This analytical method involved modeling the tube-duct interfaces as finite piston sources, which couple the acoustic field inside the main duct with the acoustic field within the HQ tubes. The acoustic field within the HQ tubes is assumed to consist of plane waves only and the acoustic field within the main duct is modeled using a higher-order mode Green's function technique.

A number of modeling simplifications were derived. These simplifications included a closed form solution for the higher-order mode model in the absence of fluid flow. A comparison with the classical plane-wave theory was also made, in which the one-dimensional model was proven to be a special case of the new higher-order model. Assuming a single-mode in both the disturbance and Green's function, the derivation of a transcendental equation allowed for the prediction of the frequencies of maximum attenuation and an additional derivation indicated attenuation at the cut-off frequencies of the modes.

The model proved that the HQ tubes were effective for reducing both the plane-wave and higher-order modes. The mechanisms associated with the reduction of multiple higher-order modes involve both reflection of the incident wave (as in the case of plane-waves) as well as spill of energy into other higher-order modes. The recombination of the energy spilled between the various modes present results in destructive interference and thus sound attenuation. This is the most important noise control mechanism of the HQ tubes in the presence of multiple modes. This noise control mechanism has been investigated using simple disturbance configurations.

The destructive interference effect is greatly affected by the relative magnitude and phase between the modes. Parametric studies have been performed to determine the influence of various system geometric parameters, such as the tube axial position, length, distance between interfaces, and cross-sectional area. It was determined that there is an optimum axial location for the maximum attenuation of all of the modes that repeats periodically down the duct. At this location, the phase of the modes leads to the best recombination of the spill of energy between modes and minimum net transmitted power. Logically, the HQ tube length is directly associated with the tube resonance frequencies and thus the frequencies of attenuation in the duct. Any change in tube length will change these frequencies of attenuation. The interface distance, while not influencing the overall transmission loss to a great degree can still be optimized. The tube cross-sectional area is limited in size by the modeling technique. This model assumes that the pressure distribution within the tubes consists of plane-waves only. Therefore, the model is limited to frequencies well below the first cut-off frequency of the side-tube transverse mode. In practice the side-tube area is limited to an area ratio of approximately 10%. In the parametric studies presented, the optimum area was found to have an area ratio of approximately 10%.

The addition of a second HQ tube array does indeed increase the attenuation benefits dramatically. Here, it was assumed that the second array of HQ tubes had the same geometry as the first array, which simplifies the study. However, a true optimization would involve the design of both the first and second array parameters. This however, is beyond the scope of this thesis. In general, the HQ system can be optimized to have unique attenuation characteristics as a function of frequency such as in noise control applications with multiple resonant frequencies. Nevertheless, the attenuation benefits need to be weighed against the cost and size constraints with the addition of more HQ tubes.

4.2 Future Research

An interesting extension of HQ tube design, for the suppression of higher-order modes, might include active control of an aspect of tube geometry in order to attain optimum attenuation of sound at a range of frequencies. For instance, in some noise control applications, it may be feasible to adjust the length of the HQ tube. Proof of the feasibility of this concept is shown in

Figure 4.1, where attenuation is shown for a range of frequencies, *2150 - 2550 Hz*, for a disturbance again comprised of the *m=0, 1, 2, 3,* and 4 modes.

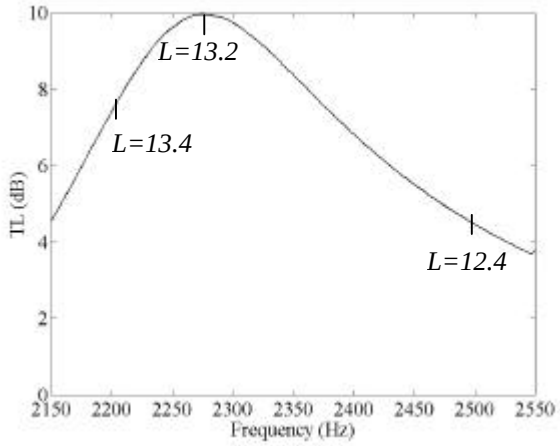

Figure 4.1 Transmission loss (dB) versus frequency (Hz) with optimized HQ tube length, *L (cm)*, at each frequency and disturbance comprised of *m=0, 1, 2, 3,* and *4* modes

In this plot, the transmission loss has been optimized at each frequency by allowing the tube length to vary. Over this 400 Hz frequency range, substantial attenuation is achieved, for example *7.4 dB* reduction is seen at *2200 Hz*, *10 dB* at *2280 Hz*, and *4.5 dB* at *2500 Hz*. This broad band reduction is accomplished by varying the HQ tube length from *12.4 - 13.4 cm*, a change in tube length of only *1.0 cm*.

However, the next logical development of this work is to include three-dimensional ducts with even more complex sound fields. Even with an increase in the sound field and system configuration complexity, the modeling technique would remain the same. Define the acoustic fields within the main-duct and side-tubes, assume that the tube-duct interfaces are finite piston sources, and couple the system by matching the acoustic pressures and particle velocities at the interfaces. It should also be kept in mind that this modeling technique can be extended to other systems, i.e. Helmholtz resonators, making modeling of complex sound fields within ducts easy to incorporate.

Bibliography

[1] Kinsler, L. E., Frey, A. R., Coppens, A. B., and Sanders, J. V., Fundamentals of Acoustics, (New York: John Wiley & Sons, 1982), pages 216-222.

[2] Bies, David A. and Hansen, Colin H., Engineering Noise Control Theory and Practice, (New York: E & FN SPON, 1998), pages 4-12.

[3] Bies, David A. and Hansen, Colin H., Engineering Noise Control Theory and Practice, (New York: E & FN SPON, 1998), pages 470-472.

[4] Tokhi, M. O. and Leitch, R. R., Active Noise Control, (Oxford: Clarendon Press; New York: Oxford University Press, 1992), pages 1-6.

[5] Harris, David A. (ed.), Noise Control Manual: Guidelines for Problem Solving in the Industrial / Commercial Acoustical Environment, (New York, Van Nostrand Reinhold, 1991), pages 10-13.

[6] Beranek, L. L. (ed.), Noise and Vibration Control, (New York: McGraw-Hill Book Co., 1971), pages 362-364.

[7] Kinsler, L. E., Frey, A. R., Coppens, A. B., and Sanders, J. V., Fundamentals of Acoustics, (New York: John Wiley & Sons, 1982), pages 237-242.

[8] Herchel, Sir John F. W., “On the Absorption of Light by Coloured Media, viewed in connexion with the Undulatory Theory”, The Philosophical Magazine, Vol. 3, No. 18, pages 401-412, Dec., 1833.

[9] Quincke, G., “Ueber interferenzapparate für schallwellen”, Annalen der Physik und Chemie, Vol. 128, pages 177-192, 1866.

[10] Stewart, G. W., “The Theory of the Herschel-Quincke Tube”, Physical Review, Vol. 31, pages 696-698, April, 1928.

[11] Selamet, A., Dickey, N. S., and Novak, J. M. (1993). “The Herschel-Quincke Tube: A Theoretical, Computational, and Experimental Investigation”, The American Society of Mechanical Engineers Winter Annual Meeting, NCA-Vol. 16, Nov. 28 – Dec. 3, 1993.

[12] Selamet, A., Dickey, N. S., and Novak, J. M., “The Herschel-Quincke Tube: A Theoretical, Computational and Experimental Investigation”, Journal of Acoustical Society of America, Vol. 96, No. 5, pages 3177-3185, Nov., 1994.

[13] Selamet, A., Radavich, P. M., and Dickey, N. S., “Multi-Dimensional Effects On Silencer Performance”, Noise-Con 94, pages 261-266, May, 1994.

[14] Selamet, A., Dickey, N. S., and Novak, J. M., “A Time-Domain Computational Simulation of Acoustic Silencers”, Journal of Vibrations and Acoustics, Vol. 117, pages 323-331, July, 1995.

[15] Selamet, A., Radavich, P. M., “Effect of Expansion Chamber On the Resonance Frequency of Side Branches and Herschel-Quincke Tubes”, Proceedings of the American Society of Mechanical Engineers, NCA-Vol. 22, pages 127-132, 1996.

[16] Selamet, A. and Easwaran, V., “Modified Herschel-Quincke tube: Attenuation and resonance for n-duct configuration”, Journal of Acoustical Society of America, Vol. 102, No. 1, pages 164-168, July, 1997.

[17] Morse, P. M., and Ingard, K. U., Theoretical Acoustics, (Princeton NJ: Princeton University Press, 1968), pages 310-312, 319-322, 500-501.

[18] Hildebrand, Francis B., Advanced Calculus for Applications, Second Edition, (Prentice Hall, Inc., 1976), pages 65-67, 653.

Appendix A – Duct Acoustics

In this appendix, the theory describing two-dimensional duct acoustics is presented. Consider the two-dimensional infinite waveguide of height *h* as shown in Figure A.1. The boundaries at *y*=0 and *y*=*h* are assumed to be rigid, which results in a sound field consisting of standing waves in the *y*-direction. The absence of boundaries along the *x*-axis allows acoustic energy to propagate and results in a sound field pattern consisting of traveling or evanescent waves [1]. With the defined waveguide geometry and boundary conditions, an expression of the acoustic pressure distribution will be derived as a solution to the acoustic wave equation.

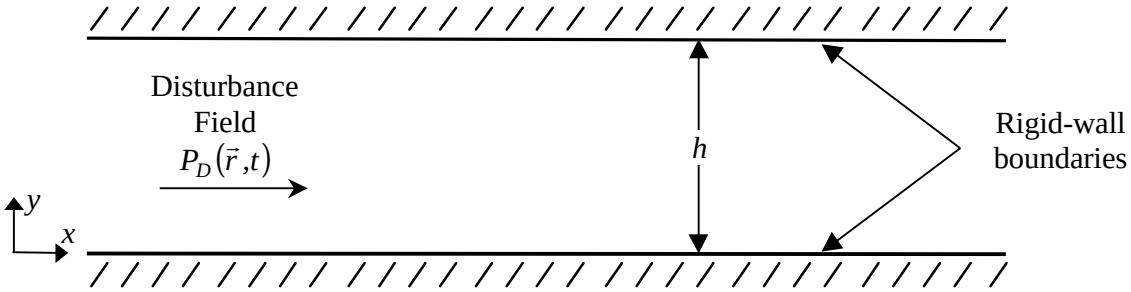

Figure A. 1. Two-dimensional infinite duct

In rectangular coordinates, the two-dimensional acoustic wave equation is a function of two spatial and one temporal variable. The equation of motion and boundary conditions are given by:

$$\frac{\partial^2 p(x,y,t)}{\partial x^2}+\frac{\partial^2 p(x,y,t)}{\partial y^2}=\frac{1}{c^2}\frac{\partial^2 p(x,y,t)}{\partial t^2}$$
$$\left.\frac{\partial p(x,y,t)}{\partial y}\right|_{y=0}=\left.\frac{\partial p(x,y,t)}{\partial y}\right|_{y=h}=0 \qquad \text{(A.1a,b)}$$

where *p(x,y,t)* is the acoustic pressure distribution and *c* is the wavespeed. In addition to the partial differential equation as shown in Equation (A.1a), the acoustic pressure must satisfy the rigid boundary conditions as given in Equation (A.1b).

By assuming simple harmonic waves of the form:

$$p(x,y,t) = P(x,y)e^{iwt} \tag{A.2}$$

and substituting Equation (A.2) into Equations (A.1a) and (A.1b), the resulting expressions are:

$$\left(\frac{\partial^2}{\partial x^2} + \frac{\partial^2}{\partial y^2} + k^2\right)P(x,y) = 0$$
$$\left.\frac{\partial P(x,y)}{\partial y}\right|_{y=0} = \left.\frac{\partial P(x,y)}{\partial y}\right|_{y=h} = 0 \tag{A.3a,b}$$

where the expression given in Equation (A.3a) is known as the time-independent Helmholtz equation, $k = w/c$ is the free-field wavenumber, and w is the frequency in radians per second. The solution to the Helmholtz equation is obtained using a separation of variables technique, which assumes a solution of the form:

$$P(x,y) = X(x)Y(y) \tag{A.4}$$

where $X(x)$ and $Y(y)$ are simply the spatial solutions in the x and y-directions, respectively. The Helmholtz equation is thus simplified to:

$$\frac{1}{X(x)}\frac{\partial^2 X(x)}{\partial X(x)^2} + \frac{1}{Y(y)}\frac{\partial^2 Y(y)}{\partial Y(y)^2} + k^2 = 0 \tag{A.5}$$

Since the first and second terms in the previous equation are a function of only the x and y variables, each of these terms must be equal to a constant. As a result, the partial differential equation can be separated into the following pair of second order differential equations:

$$\frac{d^2 X(x)}{dx^2} + k_x^2 X(x) = 0 \qquad \frac{d^2 Y(y)}{dy^2} + k_m^2 Y(y) = 0 \tag{A.6a,b}$$

where k_x^2 and k_m^2 are the constants and are related by:

$$k_x^2 + k_m^2 = k^2 \tag{A.7}$$

The solution to the *X(x)* component of the pressure expression is:

$$X(x) = K_1^{(+)} e^{-ik_x x} + K_1^{(-)} e^{ik_x x} \tag{A.8}$$

where the first and second terms represent positive and negative x-direction propagation waves with wavenumber k_x, and $K_1^{(+)}$ and $K_1^{(-)}$ are unknown constants. The solution to the *Y(y)* component is conveniently given by:

$$Y(y) = K_2 \cos(k_m y) + K_3 \sin(k_m y) \tag{A.9}$$

where K_2, and K_3 are constants of integration. The boundary conditions at $y=0$ and y=h can be applied that leads to $K_3=0$ and:

$$\sin(k_m h) = 0 \quad \Rightarrow \quad k_m = \frac{mp}{h}, \quad m = 0,1,2,... \tag{A.10}$$

Thus, the y-component of the pressure is given as:

$$Y(y) = K_2 \cos(k_m y) \tag{A.11}$$

Moreover, the axial wavenumber k_x can be solved by replacing Equation (A.10) into Equation (A.7) to give:

$$k_x^2 = \pm\sqrt{k^2 - k_m^2} \tag{A.12}$$

The propagation characteristics of the modes are given by the axial wavenumber k_x, which is given by:

$$k_x = \begin{cases} \sqrt{k^2 - k_m^2}, & k > k_m \\ -i\sqrt{k_m^2 - k}, & k < k_m \end{cases} \tag{A.13}$$

A mode will propagate for $k > k_m$ and will decay when $k < k_m$. The frequency at which this change in propagation characteristic occurs is termed the cut-off frequency for mode m. It is given for $k = k_m$ yielding:

$$w_m\left(rad/s\right) = \frac{cp}{h} m\ , \quad m = 0,1,2,3... \tag{A.14}$$

The solution for the spatial pressure distribution can now be rewritten as:

$$P(x,y) = K_4 e^{-ik_x x} F\left(k_m y\right) + K_5 e^{ik_x x} F\left(k_m y\right), \quad m = 0,1,2,... \tag{A.15}$$

where $F_m(.)$ is defined as the m^{th} acoustic mode or eigenfunction given as:

$$F\left(k_m y\right) = cos\left(k_m y\right) \tag{A.16}$$

The first and second terms in Equation (A.15) represent positive and negative x-direction propagating modes, respectively. The eigenfunctions can be described in terms of even and odd modes. Even modes ($m=0, 2, 4, \ldots$) are symmetric about the centerline of the duct, $y=h/2$, while odd modes ($m=1, 3, 5, \ldots$) are anti-symmetric about $y=h/2$. This characteristic will be useful in both simplifying and understanding analytical developments in Chapter 2 of this thesis.

Equation (A.2) can now be fully expressed in general form as the sum of a set of N_D modes propagating in the positive x-direction as:

$$p_D(\vec{r},t) = \sum_{m=0}^{N_D} A_m F_m\left(k_m y\right) e^{i(wt-k_x x)} \tag{A.17}$$

where A_m is the complex amplitude of the m^{th} *mode* (with m=0 representing the plane-wave mode). The sound field includes standing waves in the *y*-direction and travelling waves in the *x*-direction.

Appendix B – Plane Wave Analysis

In this appendix, the plane-wave acoustic theory for the Herschel-Quincke tube system is presented. This theory is considered because it is the traditional method used to describe the sound field in such a system and many publications can be found which use this basic analysis technique [10-16]. It is important to remark that this analysis is limited to one-dimensional sound fields only, i.e. plane waves. Moreover, this plane-wave analysis will be compared to the higher-order mode model, as developed in Chapter 2 when applied to the plane-wave case.

For clarity the following traditional plane-wave analysis will be presented verbatim from the publication by Selamet, et. al. [12].

> "The geometry of a Herschel-Quincke tube is shown in Fig.1, along with the nomenclature used here: *A* is the cross-sectional area, *C* the amplitude of pressure oscillations, and the subscripts + and – denote propagation in the positive and negative directions, respectively. From pressure equality at junctions I and II,
>
> $$C_{1+} + C_{1-} = C_{2+} + C_{2-} = C_{3+} + C_{3-}, \quad (1)$$
>
> $$C_{2+}e^{-ik\ell_2} + C_{2-}e^{ik\ell_2} = C_{3+}e^{-ik\ell_3} + C_{3-}e^{ik\ell 3} = C_{4+} + C_{4-}, \quad (2)$$
>
> and conservation of volumetric flow
>
> $$A_1(C_{1+} - C_{1-}) = A_2(C_{2+} - C_{2-}) + A_3(C_{3+} - C_{3-}), \quad (3)$$
>
> $$A_4(C_{4+} - C_{4-}) = A_2\left(C_{2+}e^{-ik\ell_2} - C_{2-}e^{ik\ell_2}\right) + A_3\left(C_{3+}e^{-ik\ell_3} - C_{3-}e^{ik\ell_3}\right). \quad (4)$$
>
> Equations (1) – (4) represent six equations and eight unknowns. Specifying the termination properties provides an additional equation, which allows the ratio of any two fluctuating pressure components to be determined. The transmission loss is then obtained from the ratio of the incident and transmitted waves as

$$TL = 10\log_{10}\left|\frac{C_{1+}}{C_{4+}}\right|^2 . \tag{5}$$

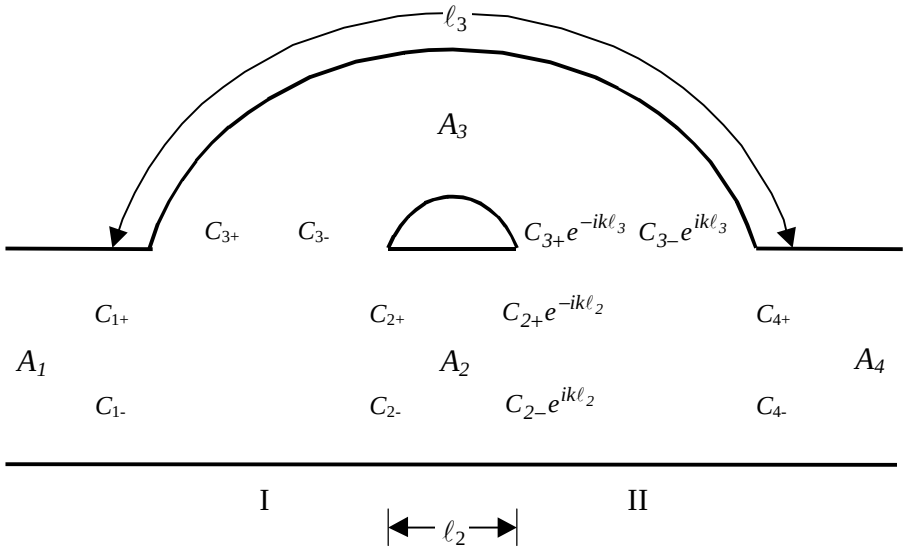

Figure B.1. Geometry and nomenclature for Quincke tube derivations.

For an anechoic termination no reflected waves are present in the exit duct. Combining C_{4-}=0 and A_4=A_1 with Eqs. (1) – (4) and rearranging yields the ratio of incident and transmitted waves as

$$\frac{C_{1+}}{C_{4+}} = -\frac{A_2 a_2 + A_3 a_3}{A_1} + \frac{\left(A_1 + A_2 f_2 + A_3 f_3\right)^2}{4A_1\left(A_2 a_2 + A_3 a_3\right)}, \tag{6}$$

where

$$a_j = \frac{e^{-ik\ell_j}}{1-e^{-2ik\ell_j}}, \quad f_j = \frac{1+e^{-2ik\ell_j}}{1-e^{-2ik\ell_j}}. \tag{7}$$

In terms of Eq. (5), the transmission loss is then given by

$$TL = 10\log_{10}\left|-\left(\frac{A_2}{A_1}a_2+\frac{A_3}{A_1}a_3\right)+\frac{\left[1+(A_2/A_1)f_2+(A_3/A_1)f_3\right]^2}{4\left[(A_2/A_1)a_2+(A_3/A_1)a_3\right]}\right|^2, \quad (8)\ldots$$

… For cases where $\ell_2 \neq \ell_3$, Eq. (8) yields resonances for

$$A_2a_2 + A_3a_3 = 0, \quad (11)$$

provided that $A_1+A_2f_2+A_3f_3 \neq 0$ at the same frequency. Inserting Eq. (7) into Eq. (11) and simplifying gives

$$\frac{\sin(k\ell_2)}{\sin(k\ell_3)} = -\frac{A_2}{A_3}, \quad (12)$$

for the resonance locations."

For a direct comparison with the higher-order mode model, two aspects of the models need to be addressed: geometry and nomenclature differences. The higher-order mode model incorporates two identical tubes, which are symmetrically located about the duct axis as compared to one used in the plane-wave model. To compensate for this, the same plane-wave analysis can be carried out with a HQ tube with twice the area, i.e. $A_3=2S$. Thus, due the linear nature of these equation sets it can be shown that one or two tubes in the plane-wave model does not make a difference. However, this is not the case when incorporating higher-order modes.

Additionally, in the higher-order mode model, the main-duct is assumed to be of constant cross-sectional area h. Thus, the cross sectional areas in the plane wave model need to be set to $A_1=A_2=A_4,=h$. The notation for both the distance between side-tube junctions and for the side tube itself for both models are related as $\ell_2=\ell$ and $\ell_3=L$, respectively. The final difference in notation refers to the complex pressure amplitudes of the incident and transmitted waves. These can be reconciled as $C_{1+} = A_0^D$ and $C_{4+} = A_0^T$.

Taking these notation differences into account, the expression as derived by Selamet, et. al. [12] for transmission loss can be rewritten (using the higher order model nomenclature) for a direct comparison with the higher-order mode model when applied to the plane-wave case. After some lengthy, but straightforward manipulation, the expression for transmission loss shown in Equation (8) can be expressed with the substitution of Equation (7) as:

$$TL = 10\log_{10}\left|\frac{4\left(\frac{1-e^{-2ikL}+AR\left(1+e^{-2ikL}-2e^{-ik\ell}e^{-ikL}\right)}{\left(1-e^{-2ik\ell}\right)\left(1-e^{-2ikl_L}\right)}\right)+AR^2}{4\left(\frac{e^{-ik\ell}}{1-e^{-2ik\ell}}+AR\frac{e^{-ikL}}{1-e^{-2ikL}}\right)}\right|^2, \quad AR=\frac{2S}{h} \qquad \text{(B.1)}$$

This should be compared with the expression found in Chapter 2 of this thesis, specifically Equation (2.51). These expressions are identical. Therefore, it is demonstrated that the plane-wave analysis is indeed a special case of the higher-order mode model developed in this thesis.

Appendix C – The Green's Function

In this appendix, the derivation of the Green's function is presented. The Green's function is used in the modeling of the HQ tubes as piston sources at the tube-duct interfaces, as presented in Section 2.1 of this thesis. Thus, to model the HQ tubes it is necessary to know the sound field within the duct for a simple-source located within the duct. The Green's function represents this sound field [17].

The sound field generated by a simple source located at a position (x_0,y_0) in a two-dimensional infinite duct has to satisfy the following differential equation:

$$\left[\frac{\partial^2}{\partial x^2}+\frac{\partial^2}{\partial y^2}+k^2\right]G(x,y|x_0,y_o)=-\delta(x-x_0)\delta(y-y_0) \qquad \text{C.1}$$

and the rigid-wall boundary conditions. In Equation (C.1), G(.) is the Green's function which is the solution to the non-homogenous time-independent form of the acoustic wave equation forced by a Dirac delta function. The homogenous solution to the wave equation yielded the acoustic mode shapes and eigenvalues which were derived in detail in Appendix A. Here the Green's function is expressed as a linear combination of the acoustic modes. The boundary conditions are thus satisfied automatically. Then, the Green's function solution is assumed to have the form:

$$G=\sum_n F_n(x)F_n(y) \qquad \text{C.2}$$

which is a summation of a series of eigenfunctions and the function $F_n(x)$ representing the variation along the duct of the pressure. By inserting Equation (C.2) into Equation (C.1), multiplying by $F_{n'}(y)$, and integrating over the duct cross-section, Equation (C.1) becomes:

$$\sum_n \int_0^h F_n(y)F_{n'}(y)dy\,\frac{\partial^2}{\partial x^2}[F_n]+\sum_n F_n\int_0^h F_{n'}(y)\frac{\partial^2}{\partial y^2}[F_n(y)]dy+k^2\sum_n F_n\int_0^h F_n(y)F_{n'}(y)dy=$$
$$-d(x-x_0)\sum_n\int_0^h d(y-y_0)F_{n'}(y)dy \qquad \text{C.3}$$

in which care is taken to distinguish between the summation orders in the previous integral. This is accomplished using the notation *n'* to indicate the summation order of the eigenfunction which is multiplied through the equation. Using the orthogonality properties of the modes, the integrals on the left-hand side in Equation (C.3) become :

$$\int_0^h F_n(y)F_{n'}(y)dy=\begin{cases}\int_o^h \cos(k_n y)\cos(k_{n'}y)dy=0, & n\neq n'\\ \int_0^h \cos^2(k_n y)dy=\frac{h}{2}, & n=n'\\ \int_0^h dy=h, & n=n'=0\end{cases} \qquad \text{C.4}$$

and:

$$\int_0^h F_{n'}(y)\frac{\partial^2}{\partial y^2}[F_n(y)]dy=-k_n^2\int_0^h F_{n'}(y)F_n(y)dy \qquad \text{C.5}$$

Using the shifting property of the Dirac delta function [18], the integral on the right-hand side in Equation (C.3) becomes:

$$\int_0^h d(y-y_0)F_{n'}(y)dy=F_{n'}(y_0) \qquad \text{C.6}$$

Therefore, Equation (C.3) can be reduced to an ordinary differential equation of the form:

$$\left[\frac{d^2}{dx^2}+k_x^2\right]F_n(x)=-\frac{F_{n'}(y_0)}{L}d(x-x_0),\quad L_n=\begin{cases}h, & n=0\\ h/2, & n\neq 0\end{cases} \tag{C.7}$$

where:

$$k_x^2=k^2-k_n^2 \tag{C.8}$$

Due to the discontinuity at x_0, the solution to the differential equation shown in Equation (C.7) will be different at each side of x_0. On the positive side of x_0, i.e. $x>x_0$, the solution will be of the form $e^{-ik_x(x-x_0)}$. On the negative side of x_0, i.e. $x<x_0$, the solution will take the form $e^{ik_x(x-x_0)}$. Since the overall solution must be continuous across x_0, it can be written as:

$$F_n(x)=Ce^{-ik_x|x-x_0|} \tag{C.9}$$

where the constant C must be determined such that $|x-x_0|=x-x_0$ for $x>x_0$ and $|x-x_0|=x_0-x$ for $x<x_0$. Therefore, $F_n(x)$ has a discontinuity in slope across $x=x_0$ and the magnitude of this discontinuity, namely C, can be found by taking the limit as $a \to 0$ in the integral over x from x_0-a to x_0+a of Equation (C.7):

$$\int_{x_0-a}^{x_0+a}\frac{d^2F_n(x)}{dx^2}dx+k_x^2\int_{x_0-a}^{x_0+a}F_n(x)dx=-\frac{F_{n'}(y_0)}{L}\int_{x_0-a}^{x_0+a}d(x-x_0)dx \tag{C.10}$$

which reduces to:

$$\left.\frac{dF_n(x)}{dx}\right|_{x_0-a}^{x_0+a}+k_x^2\,2aF_n(x)=-\frac{F_{n'}(y_0)}{L} \tag{C.11}$$

and in the limit to:

$$\lim_{a\to 0}\left[\left(\frac{dF_n(x)}{dx}\right)_{x_0+a}-\left(\frac{dF_n(x)}{dx}\right)_{x_0-a}\right]=-\frac{F_{n'}(y_0)}{L_n} \qquad \text{C.12}$$

For x_0+a the slope of the solution is $-ik_xCe^{-ik_xa}$ and similarly for x_0-a the slope of the solutions is $ik_xCe^{-ik_xa}$. Therefore, Equation (C.12) becomes $C=-iF_n(y_0)/2L_nk_x$ yielding the solution to $F_n(x)$ as:

$$F_n(x)=\frac{-i}{2}\sum_{n=0}^{N_g}\frac{F_n(y_0)}{L_nk_x}e^{-ik_x|x-x_0|} \qquad \text{C.13}$$

and the full solution to the Green's function as:

$$G(\vec{r}|\,\vec{r}_0)=\frac{-i}{2}\sum_{n=0}^{N_g}\frac{F_n(y)F_n(y_0)}{L_nk_x}e^{-ik_x|x-x_0|} \qquad \text{C.14}$$

This Green's function solution represents the sound field within the duct for a simple source also located within the duct. In order to model the HQ tubes, the tube-duct interfaces are described as piston sources. The sound field generated by a piston source is computed by integrating the Green's function over the cross-section of the piston.

In this integration, each piston source is modeled locally with coordinate x_i as shown in Figure C.1 for three possible integration scenarios. When the observation and source location are the same, as is the case with $\tilde{G}_{11}$, the integration is carried out as follows:

$$\tilde{G}_{11}=2\int_0^{S/2}G_{11}dx_1=-i\int_0^{S/2}\sum_{n=0}^{N_g}\frac{F(k_nh)^2}{L_nk_x}e^{-ik_x|x_c-(x_c-x_1)|}dx_1=\sum_{n=0}^{N_g}\frac{F(k_nh)^2}{L_nk_x^2}\left(e^{-ik_x\frac{s}{2}}-1\right) \qquad \text{(C.15)}$$

where the limits of integration have been changed to twice the limit from *0* to *S/2* and is valid as long as $|-x_1| > 0$, which is always true.

The second integration case occurs when the source is upstream of the observation location, for example $\tilde{G}_{21}$ is given as:

$$\tilde{G}_{21} = \int_{-S/2}^{S/2} G_{21} dx_1 = -\frac{i}{2} \int_{-S/2}^{S/2} \sum_{n=0}^{N_g} \frac{F(k_n h)^2}{L_n k_x} e^{-ik_x|(x_c+\ell)-(x_c-x_1)|} dx_1 = \sum_{n=0}^{N_g} \frac{F(k_n h)^2}{L_n k_x^2} e^{-ik_x \ell} \sin\left(k_x \frac{s}{2}\right) \quad \text{(C.16)}$$

which is valid as long as $l > x_1$.

The third possible integration case occurs when the source is downstream of the observation location, for example $\tilde{G}_{34}$ is given as:

$$\tilde{G}_{34} = \int_{-S/2}^{S/2} G_{34} dx_4 = -\frac{i}{2} \int_{-S/2}^{S/2} \sum_{n=0}^{N_g} \frac{F(k_n 0)^2}{L_n k_x} e^{-ik_x|x_c-(x_c+\ell-x_4)|} dx_4 = \sum_{n=0}^{N_g} \frac{F(k_n 0)^2}{L_n k_x^2} e^{-ik_x \ell} \sin\left(k_x \frac{s}{2}\right) \quad \text{(C.17)}$$

which is valid as long as $l > x_4$..

Thus from the symmetry of the problem, there are really only two cases to consider and the integrated Green's functions can be written in general form as:

$$\tilde{G}_{rs} = \sum_{n=0}^{N_g} \frac{F(k_n y_r) F(k_n y_s)}{L_n k_x^2} \left(e^{-ik_x \frac{s}{2}} - 1 \right), \quad x_r = x_s$$
$$\tilde{G}_{rs} = -i \sum_{n=0}^{N_g} \frac{F(k_n y_r) F(k_n y_s)}{L_n k_x^2} e^{-ik_x \ell} \sin\left(k_x \frac{s}{2}\right), \quad x_r \neq x_s \quad \text{(C.18a,b)}$$

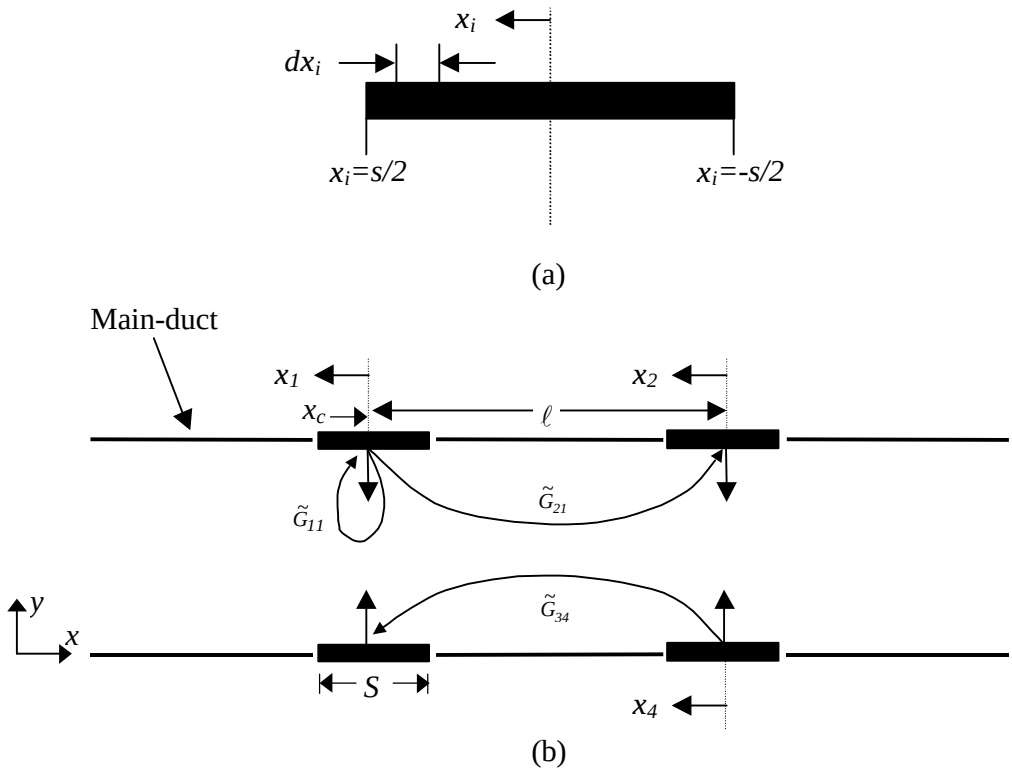

Figure C.1. Integration of Green's functions; (a) piston source local coordinate system and (b) examples of integrated Green's function notation

Vita

Lori Brady was Born on 30 May 1973 in Worcester, Massachusetts. She spent her childhood there, graduating from Holy Name Central Catholic High School in May 1991. She began her undergraduate studies the following September at the University of Massachusetts, at Amherst and graduated in 1996 with a Bachelor of Science degree in Mechanical Engineering. She then began work toward a Master of Science degree in Mechanical Engineering at Virginia Tech under the guidance of Professor Ricardo Burdisso in the Vibration & Acoustics Laboratories.